# Hardware-in-the-Loop Dynamic Wind Tunnel Investigation of Slung Loads Dynamics with Application to Active Cargo Hook Stabilization of an M119 Howitzer

**Reuben Raz** Researcher
**Aviv Rosen*** Researcher
Tel-Aviv University
Tel-Aviv, Israel

**Samuel J. Nadell** Research Engineer
Universities Space Research Assoc.
Moffett Field, CA

**Luigi Cicolani** Research Engineer
San Jose State Research Foundation
Moffett Field, CA

**Joseph F. Horn** Professor
**Jacob Enciu** Assistant Research Professor
**Zhouzhou Chen** Graduate Student
Department of Aerospace Engineering, The Pennsylvania State University
University Park, PA, USA

**Mark B. Tischler**
Senior Technologist
U.S. Army CCDC, AvMC, Technology Development Directorate
Moffett Field, CA, USA

**Kenny K. Cheung**
Chief Software Architect
Universities Space Research Association
Moffett Field, CA

## ABSTRACT

A new hardware-in-the-loop (HIL) dynamic wind tunnel setup is used to study the behavior of a slung load at high speeds and methods of stabilizing problematic loads. The main element of the setup is a movable cargo hook. In addition the cable angles, model spatial attitude, and hook force are measured continuously. All the measurements are fed into a computer that calculates the cargo hook resultant motion in real-time by summing the rotorcraft angular motion effects (not used in the current study) and the hook motion relative to the rotorcraft fuselage. The computer output includes motion commands to the hook. The slung loads are two configurations of an M119 howitzer: folded and ready for firing. Initial wind tunnel studies showed that these loads exhibit significant LCO (Limit Cycle Oscillations) and severe instabilities at high speeds. Frequency sweep tests are used to derive dynamic models of the slung loads. These models are used to develop two controllers based on an Active Cargo Hook (ACH) approach. These controllers were implemented, tested, and studied. It was shown that both were able to suppress LCO and stabilize the slung loads along the entire airspeed range.

## NOTATION

| | |
|---|---|
| C | controller compensation |
| d | lag parameter ($s^{-1}$) |
| G | controller filter |
| K | controller gain (mm/deg) |
| $K_p$ | Pendulum transfer function gain (deg/mm) |
| p | washout parameter ($sec^{-1}$) |
| X, Y, Z | wind tunnel axes: local vertical axes with X aligned into the wind and Z points downwards. |
| x | longitudinal hook position (mm from a central position) |
| $x_{cmd}$ | longitudinal external command to ACH (mm) |
| $x_{tot}$ | longitudinal total command into ACH actuator, (mm) |
| $\delta x$ | longitudinal feedback command to ACH (mm) |
| y | lateral hook position (mm from a central position) |
| $y_{cmd}$ | lateral external command to ACH (mm) |
| $\delta y$ | lateral feedback command to ACH (mm) |
| $\zeta_p$ | pendulum damping ratio |
| $\theta_C$ | longitudinal cable angle (deg) |
| $\theta_{dist}$ | external longitudinal cable angle disturbance (deg) |
| $\theta'_C$ | longitudinal cable angle input to controller (deg) |

* Professor Emeritus, Technion-Israel Institute of Technology, Haifa

This is work of the U.S. Government and is not subject to copyright protection in the U.S. Distribution statement A. Approved for public release; distribution is unlimited.

Presented at the Vertical Flight Society's 76th Annual Forum & Technology Display, Virginia Beach, October 6-8, 2020. Copyright © 2020 by the Vertical Flight Society. All rights reserved.

| | |
|---|---|
| $\theta_T$ | trail angle – mean steady state longitudinal cable |
| $\tau_a$ | actuator time constant (sec) |
| $\phi_C$ | lateral cable angle (deg) |
| $\psi$ | load yaw rotation about the vertical from the direction of flight (deg) |
| $\omega_{gc}$ | gain crossover frequency (rad/s) |
| $\omega_p$ | pendulum frequency (rad/s) |
| $\tau$ | time delay in the pendulum dynamics (sec) |
| $[y/x]$ | symbolizes frequency response with y as output and x as input |

**Acronyms**

| | |
|---|---|
| ACH | active cargo hook |
| CAF | cable angle feedback |
| CCDC | combat capabilities development command |
| DM | time delay margin (s) |
| FS | full scale |
| GM | gain margin |
| HIL | hardware-in-the-loop |
| LCAF | lagged cable angle feedback |
| LCO | limit cycle oscillations |
| PM | Phase margin |
| WT | wind tunnel |

## INTRODUCTION

Slung loads dynamics is a complicated coupled phenomenon that is determined by the inertial and aerodynamic characteristics of the load and helicopter, method of connecting the load to the helicopter, and pilot behavior. In many cases the helicopter/slung-load/pilot system exhibits instabilities that lead to a reduction of the maximum allowed airspeed of the system in order to avoid risks. The usual procedure of slung load clearance for flight with a certain helicopter requires many hours of flight testing (Ref. 1). Previous investigations (Refs. 2-4) showed that wind tunnel tests can be used in order to reduce the time, cost and risk of slung load clearance. It was also shown that dynamic wind tunnel tests are very useful in developing and verifying means for stabilizing problematic loads. Passive stabilization by rigid and fabric fins (Refs. 2-7) and active stabilization by inducing load rotation (Ref. 8) were demonstrated in dynamic wind tunnel tests. Furthermore, static and dynamic wind tunnel testing of slung load models can be used to develop and validate simulations of a helicopter/slung-load/pilot system (Ref. 9). A balanced approach of combining simulation, wind tunnel testing, and flight tests is the best approach to clear new loads for flight and develop means to cope with instabilities.

In almost all of the previous wind tunnel tests of slung load dynamics, the models were connected (by slings) to a fixed point (hook) on the tunnel ceiling (e.g. Refs. 2-4). Thus, those tests did not include the important influences of the hook motions due to helicopter response to pilot commands, atmospheric disturbances, or the response of the helicopter to the force that is applied on it by the slung load (through the hook). Instead, these influences were investigated by numerical simulations of the coupled helicopter-slung load system (Refs. 9-12). While dynamic simulation models of helicopters exist in many cases, the development of dynamic numerical simulations of slung loads and their verification, usually require long, tedious and expensive procedures. Thus, it would be very useful to develop a capability of wind tunnel testing of slung loads models, where it would also be possible to include the hook motions. A recent research project on dual lift trim, maneuvers, stability and control (Ref. 13) included wind tunnel tests of a pendant dual lift system. A special wind tunnel rig was designed and built to represent the two helicopters hooks, as well as the suspension and load below the hooks. Four of the six degrees of freedom of motion of the hooks were modeled and operated by open and closed loop control systems. Wind tunnel tests showed the capability of a closed loop control system to significantly reduce the differences in load distribution between the two helicopters during maneuvers.

As Future Vertical Lift (FVL) rotorcraft are designed to be operated at airspeeds in excess of 200kts, a research program for the development of active stabilization methods of external loads during high speed flight was recently initiated by CCDC Aviation and US Army Technology Development Directorate. Specifically, the use of cable angle feedback (CAF) to the rotorcraft primary flight control system and the feasibility of using an Active Cargo Hook (ACH) were both studied as potential techniques to providing load damping at high speed flight. Early work on the stabilization of slung loads at low speeds included Refs. 14, 15. More recently CAF was shown in simulation (Ref. 16) as capable of providing load damping in hover and low-speed flight by the use of relative cable angle measurements and lagged relative cable angle feedback (LCAF). In Ref. 17, a controller based on rate and angle feedback was designed and flight tested on a UH-60 RASCAL in hover and low-speed. Recently, load stabilization in high speed flight using a LCAF controller was demonstrated using nonlinear simulations (Ref. 18). An ACH for low-speed load stabilization was also reported in Ref. 19. A hybrid control solution consisting of an ACH and a flight

control load stabilization mode in the primary control system using LCAF was developed. The system was flight tested (Ref.20) on an H-6 flying test bed where the hook was mounted on a rail system underneath the helicopter and could be moved longitudinally and laterally based on lagged cable angle feedback. It demonstrated significant increase in load damping during low-speed flight. The concept of using an ACH for load stabilization in high-speed flight was later studied in Refs. 21-22. Nonlinear simulations of a UH-60 Black Hawk carrying a CONEX with stabilization fins showed that a full-state feedback quadratic controller for the ACH was successful in providing system stability throughout the target flight speed envelope.

The present paper will describe the development and use of a new wind tunnel setup to study the high-speed carriage of slung loads. This setup is capable of real time modeling of the hook motions, including motions that are results of the response of the helicopter to the dynamic forces that are applied by the slung load through the hook. First, the paper describes a new wind tunnel rig and the new slung load models that were investigated. Then results of initial open loop dynamic tests of the new slung load models that were tested, using the new wind tunnel setup, will be presented. These tests included trim, maneuvers, and frequency sweeps at increasing wind tunnel speeds. The initial test results were used to identify transfer function models of the slung load dynamics and the transfer functions were used to design control laws for an ACH that will suppress LCO (Limit Cycle Oscillations) and instabilities that appear at high speeds. Two controllers were developed based on simulation models obtained using system identification. These controllers were implemented in the wind tunnel setup. The implementation of the controllers required real time hardware-in-the-loop (HIL) procedures. At any moment load motion, cable angles, and the force that the load applied on the hook were measured. This data was fed into a computer that calculated the commands to move the hook. Both controllers were successful in stabilizing the loads over the entire speed range.

## WIND TUNNEL TEST SET-UP

The slung loads that were tested are two carrying configurations of the M-119 Howitzer (see Figure 1): (a) with the gun barrel folded back and (b) with the gun barrel in the 20 deg. firing position. These configurations are currently limited to maximum airspeeds of 110 kts and 120 kts, respectively, by the multiservice helicopter sling load rigging procedures for single-point loads (Ref. 1). The wind tunnel models were connected by slings that model the standard military 4-legged sling set, and rigged to the models in accordance with Ref. 1. The wind tunnel models are 20:1 scaled plastic models that were manufactured by Gamla Model Makers. Model weight and center of gravity (cg) location were adjusted for dynamic similarity to the full-scale M-119 (based on Froude scaling).

The tests were carried out at the Aerodynamic Laboratory of Tel-Aviv University. The wind tunnel cross-section is 61x150 cm (width x height) and the speed range is 4-60 m/s. The test system includes a slung load model that is connected through slings to a moving hook. The motion of the hook is in general a result of the helicopter fuselage motion due to the combination of pilot commands, autopilot commands, atmospheric disturbances, and cable forces that are transferred from the load to the fuselage (through the hook). In addition, the motion can describe an ACH. In this study only the ACH was simulated. The moving hook has two linear degrees of freedom: longitudinal (along the flow direction of the wind tunnel) and lateral (from wall to wall of the wind tunnel). Usually vertical motions have only minor influences on the system dynamics and stability.

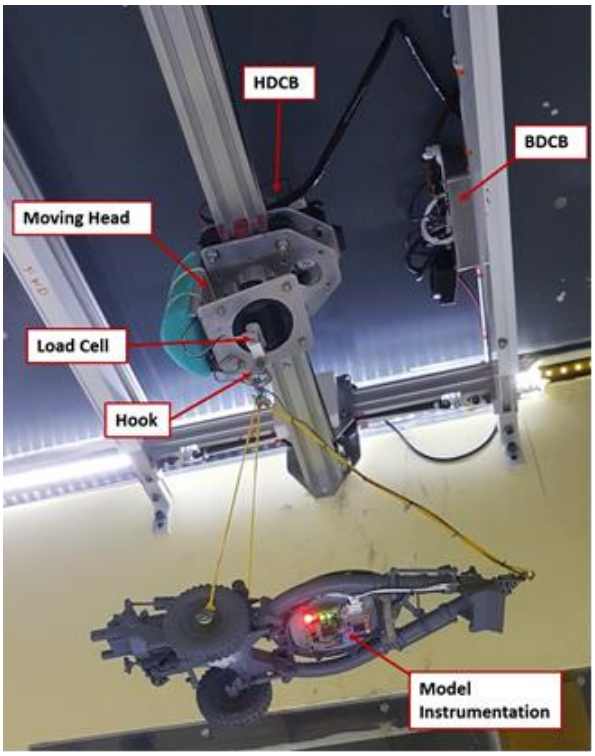


**(a)**

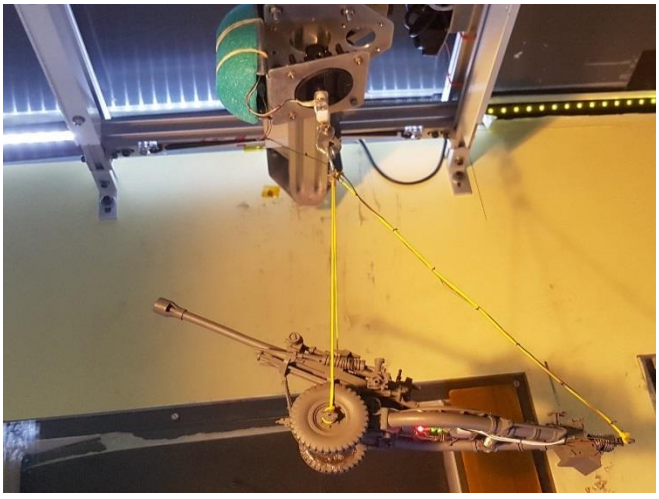

**(b)**

**Figure 1.The two models in the wind tunnel: (a) Folded position (b) Firing position.**

A frame made of standard extruded aluminum is attached to the tunnel ceiling (see Figure1). Rollers that slide on the frame allow for the longitudinal and lateral motions, which are commanded by electric step motors with toothed pulleys and timing belts. A small instrumentation package is installed beneath the model firing platform (shown in Figure1a) to measure the 3 components of: linear acceleration, angular rate, and the local magnetic field. The angular attitude and heading are estimated from these measurements. The Head Data Collection Box (HDCB) that is installed on the moving head (see Figure1a) collects the data from the model instrumentation package and also data from the following sensors: 2 potentiometers that measure the cable angles, a load cell that measures the combined force of all four cables and four IR sensors that measure the position of the hook. All the above described collected data is transmitted to a laptop outside the wind tunnel, which controls the entire test, displays selected test parameters in real time, and records the tunnel speed. Figure 1a also shows the Base Data Collection and Control Box (BDCB) that communicates with the laptop to receive commands, controls the step motors, and sends real-time data to the laptop.

## OPEN LOOP TESTS

The first phase of the tests included open loop tests to identify a model of the load response to ACH commands. A typical test started with various frequency sweeps in the longitudinal (X) and lateral (Y) directions, at zero wind speed. Then the wind speed was increased by steps of 1 m/s, from 6 m/s (52 kts FS) up to instability or a trailing angle exceeding 45 degrees. The discussion in this section will refer to FS airspeed to make clear that the two configurations of the M119 face LCO and stability problems within the airspeed range of the Future Vertical Lift (FVL) rotorcraft (200kts). At each speed the system was allowed to stabilize for two minutes. Then sharp step inputs in the X-direction were applied, followed by similar inputs in the Y-direction. At selected speeds frequency sweeps in the X- and Y-directions were performed. At the end, runs of continuously increasing the wind speed, up to its maximum value, and then continuously decreasing the speed, were carried out. All the parameters were recorded continuously and typical results will be presented in this section.

The steady state cg position of the load can be given in terms of the longitudinal and lateral cable angles relative to axes aligned with the direction of flight, $\phi_C$ , $\theta_C$ , which are illustrated in Figure 2 (first pitch, positive forward, and then roll, positive left). Although the load is in continual motion and in some cases is unstable, the steady state cable angles could be calculated from periods with small load motions around a mean value. In addition, the M119 also adopted a steady yaw angle, $\psi$, unlike many loads that undergo large yaw oscillations, in some cases enough to continually wind up and unwind the sling. Regarding those yawing loads, the ACH provides no control over load yaw.

Figure 3 shows the model attitude angles (pitch, roll, and yaw), cable angles, and the ratio between the cable force and load weight, of the folded configuration. Tunnel speed was increased rapidly from 0 to 10 m/s (87 kts FS) in a range where the load is very stable, and slowly from 10 to 23 m/s (87 to 200 kts FS). The longitudinal cable angle reaches the aft safety limit (-45 deg) at 200 kts FS. It can be seen that above 113 kts FS there are LCO about the mean values of the load angles, cable angles, and hook force. The results show that there are relatively small offsets from zero in the mean lateral cable angle and load's roll and yaw angles. Knowledge of the hook force magnitude, as well as the cable angles, allowed calculation of the load lift and drag from the force balance equations. These calculations showed that the folded configuration has a significant negative lift (reaching -0.75 g at 200 kts FS) that increases the apparent weight of the load.

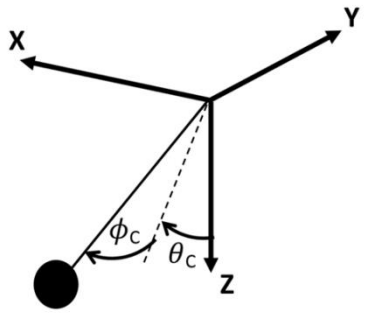


**Figure 2. Longitudinal and lateral cable angles.**

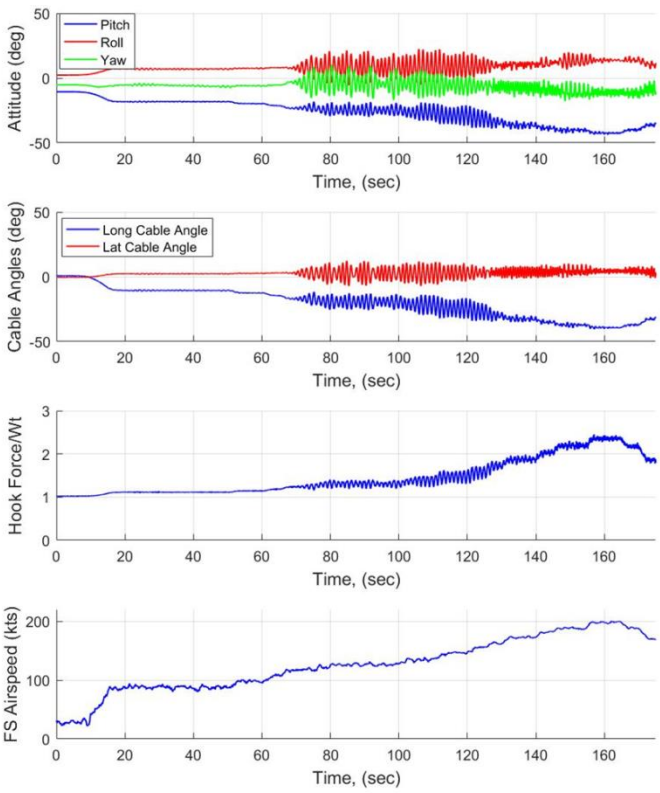


**Figure 3. The model attitude, cable angles, and ratio of hook force to weight, of the folded configuration during a slow increase of the wind tunnel speed.**

Figure 3 shows that in the case of the folded configuration the increase in the hook force at the maximum speed is almost 130% compared to the hook force in hover. Such a significant increase in the hook force becomes a factor to consider when extending the speed envelope of slung load operations beyond their current limits. Figure 4 shows the mean cable angles and load yaw angle of the folded configuration, as functions of the full scale airspeed.

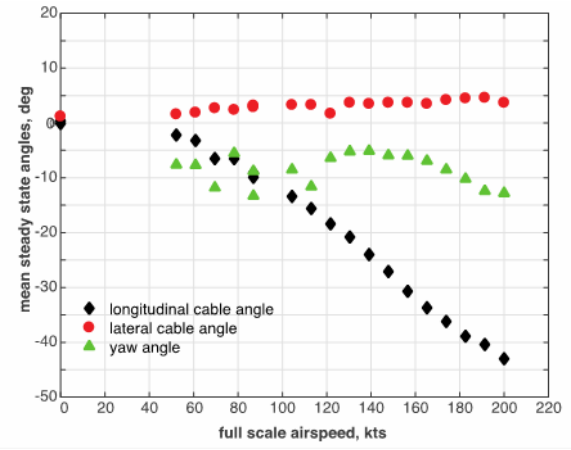


**Figure 4. Mean cable angles and load yaw angle of the folded configuration as functions of the full scale airspeed.**

Figure 5 shows, for the firing configuration, the same data that was presented in Figure 3 for the folded one. It is interesting to note that the load pitch angle in this case, for a certain wind tunnel speed, is much smaller than in the case of the folded configuration. On the other hand the magnitudes of the load roll and yaw angles, for a certain wind tunnel speed, are significantly larger than in this case of the folded configuration. The different orientation of the load in this case results in a much smaller negative lift force, than the negative lift force in the case of the folded configuration. Therefore Figure 5 does not show the significant increase of hook force with speed that was shown in Figure 3. Another clear difference between the two configurations is that while in the case of the folded configuration LCO were evident above 113 kts FS, similar LCO do not appear in the case of the firing configuration. Nevertheless, at a speed of 130 kts FS oscillations of all the measured parameters appear and grow relatively fast, reaching amplitudes that require an immediate reduction of the tunnel speed. Thus for the firing configuration the load became unstable before the trail angle limit was reached.

The larger steady state load yaw angles for the firing configuration are probably an indication that the directional stability of the firing configuration is small. This is probably the reason that in certain tests of the firing configuration there occurred a discontinuous sign change in yaw angle just above 80 kts FS, thought to reflect a switch between stable trim headings on either side of the direction of flight. Figure 6 presents the mean cable angles and load yaw angle of the firing configuration, as functions of the full scale airspeed, in a test where there was a switch between stable trim headings. It is also shown that the discontinuous sign change in the yaw angle results in a smaller discontinuity in the lateral cable angle.

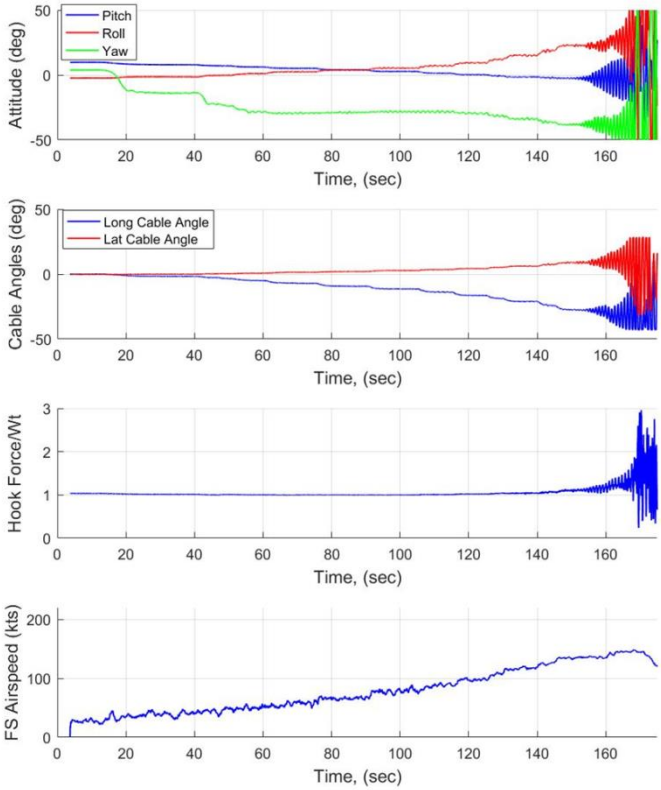


**Figure 5. The model attitude, cable angles, and ratio of hook force to weight, of the firing configuration during a slow increase of the wind tunnel speed.**

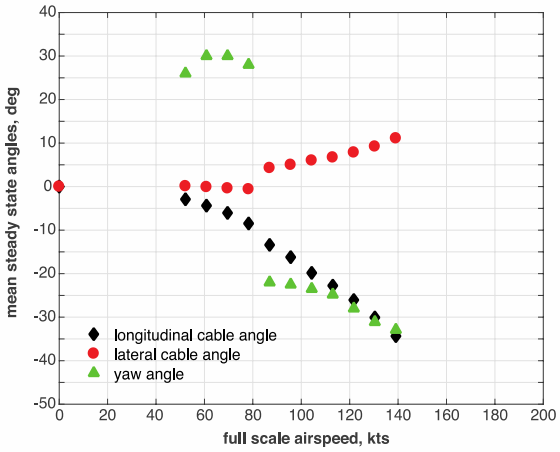


**Figure 6. Mean cable angles and load yaw angle of the firing configuration as functions of the full scale airspeed.**

## IDENTIFICATION OF PENDULUM DYNAMICS

The control system design will be based on linearized models of the pendulum oscillations of the load around its steady state position. Linearized models of the pendulum dynamics were identified from frequency sweep tests in which

the hook is driven through the range of frequencies of interest (Ref. 23). Table 1 gives the expected simple pendulum modal frequency for the suspension rigged according to the Multiservice Helicopter Sling Load manual (Ref. 1) and scaled for the tunnel, the range of airspeeds of interest (out to 200 kts FS) and appropriate choices of the sweep parameters. The actuator limits are those imposed in the sweep design to avoid saturating a limit and are within the limits of the actuator of the tunnel rig.

**Table 1. Test plan parameters for the open loop tests**

| Item | Model Scale | Full Scale |
|---|---|---|
| Pendulum length | 273.6 mm | 18.0 ft |
| Simple pendulum frequency | 6.00 rad/s | 1.34 rad/s |
| Sweep frequency range | .22 to 53.7 rad/s | .05 to 12 rad/s |
| Sweep amplitude | 9, 15, 30 mm | 0.6, 1.0, 2.0 ft |
| Sweep duration | 44.7 sec | 200 sec |
| Desired airspeed range | 0 to 23 m/s | 0 to 200 kts |
| Hook position limits | ±80 mm | |
| Hook rate limits | ±100 mm/s | |
| Note: Froude scaling, scale = 20 | | |

Time histories of the customized test sweep and a sample case response are shown in Figure 7. Input amplitude was selected at 9 mm, well within the hook position limits. At the higher frequencies amplitude is reduced as a function of frequency to avoid exceeding the hook rate limit, starting at 11.4 rad/s in the test sweep. Initial results at amplitudes of 15 and 30 mm did not show any significant differences in frequency responses from the 9 mm amplitude that would reflect significant increases in nonlinearity with amplitude. Following the tests, it was found that the motor-hook assembly did not respond to commanded frequencies above 25 rad/s limited by the mass of the hook assembly and load. However, the actuator frequency response showed excellent coherence, reflecting a highly linear input/output response and excellent signal to noise ratio out to 20 rad/s which provided ample frequency range around the pendulum mode for its identification. In Figure 7 the longitudinal cable angle oscillations are seen to center around the trail angle of the test speed. In the figure, the pendulum does not respond at low input frequencies and begins responding when the input frequency approaches the pendulum frequency.

Frequency responses for the pendulum dynamics, $[\phi_C/y]$ and $[\theta_C/x]$, were generated and a transfer function model was fitted to the responses using the CIFER® (Ref. 23) package of frequency domain analysis utilities widely used for system identification in aeronautical applications. The identification model for the simple pendulum dynamics is:

$$TF = \frac{K_p s^2}{\left(s^2 + 2\zeta_p \omega_p s + \omega_p^2\right)} e^{-s*\tau} \quad (1)$$

where the time delay, $\tau$, is introduced to account for unknown delays in the system. The sample frequency response and fit in Figure 8 shows the typical magnitude peak and 180 deg phase shift at the pendulum frequency. The model was identified over the range of 2 to 20 rad/s where coherence was generally good. This same range was used for all cases. Identification costs below 100 are considered good (Ref. 23); the cost for the sample case was 141 but it is apparent from the figure that the fit is credible.

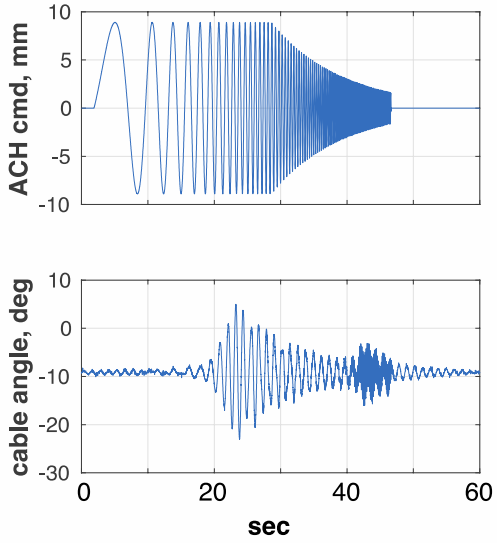


**Figure 7. Test sweep and sample case cable angle response (10 m/s, folded, longitudinal cable angle).**

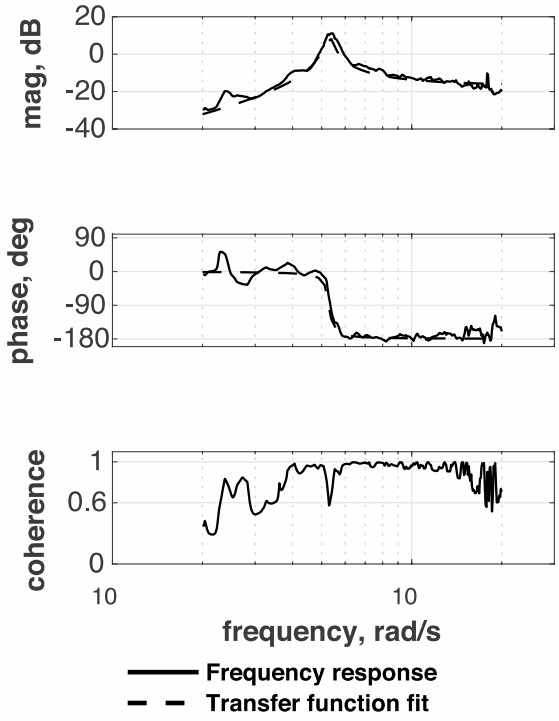


**Figure 8. Sample case frequency response and transfer function fit (10 m/s, folded, longitudinal cable angle).**

Tables 2 and 3 summarize the model results for the folded and firing configurations, respectively. For the folded configuration good models of the longitudinal pendulum mode were obtained out to 174 kts FS, above which the mode becomes unstable. Good models were obtained for the lateral pendulum mode out to 122 kts FS above which the response is swamped by large lateral-directional LCO or is unstable. The roots are nearly independent of airspeed and very lightly damped ($\zeta_p$ = .005 to .06) in the stable region. Similarly, the model for the firing configuration is nearly independent of airspeed and very lightly damped. In this case, above 122 kts FS, the sweep excited divergent oscillations on both axes.

**Table 2. Identified pendulum models, folded configuration**

| WT Speed (m/s) | FS Speed (kts) | $K_p$ | $\zeta_P$ | $\omega_p$ (rad/s) | $\tau$ (sec) | cost |
|---|---|---|---|---|---|---|
| Longitudinal, [$\theta_C$ / x] | | | | | | |
| 0 | 0 | -.172 | .010 | 5.55 | .019 | 149 |
| 6 | 52. | -.180 | .017 | 5.46 | .013 | 36 |
| 8 | 70 | -.191 | .022 | 5.39 | .013 | 28 |
| 10 | 87 | -.173 | .019 | 5.33 | .014 | 141 |
| 12 | 104 | -.176 | .022 | 5.24 | .013 | 64 |
| 14 | 122 | -.172 | .037 | 5.19 | .007 | 166 |
| 16 | 139 | -.210 | .027 | 5.27 | .010 | 40 |
| 18 | 157 | -.158 | .041 | 5.45 | .007 | 50 |
| 20 | 174 | -.174 | .033 | 5.54 | .004 | 83 |
| Lateral, [$\phi_C$ /y] | | | | | | |
| 0 | 0 | .176 | .006 | 5.48 | .022 | 17 |
| 6 | 52. | .194 | .017 | 5.59 | .020 | 22 |
| 8 | 70 | .187 | .017 | 5.62 | .020 | 18 |
| 10 | 87 | .193 | .020 | 5.70 | .019 | 48 |
| 12 | 104 | .214 | .040 | 5.86 | .018 | 108 |
| 14 | 122 | .225 | .047 | 6.19 | .021 | 183 |

**Table 3. Identified pendulum models, firing configuration**

| WT Speed (m/s) | FS Speed (kts) | $K_p$ | $\zeta_P$ | $\omega_p$ (rad/s) | $\tau$ (sec) | cost |
|---|---|---|---|---|---|---|
| Longitudinal, [$\theta_C$ /x] | | | | | | |
| 0 | 0 | -.152 | .010 | 5.51 | .014 | 58 |
| 6 | 52 | -.152 | .024 | 5.60 | .014 | 71 |
| 8 | 70 | -.169 | .027 | 5.58 | .014 | 92 |
| 10 | 87 | -.175 | .027 | 5.61 | .018 | 114 |
| 12 | 104 | -.170 | .041 | 5.73 | .010 | 81 |
| 14 | 122 | -.159 | .058 | 6.06 | .006 | 162 |
| Lateral, [$\phi_C$ /y] | | | | | | |
| 0 | 0 | .176 | .007 | 5.45 | .025 | 23 |
| 6 | 52 | .183 | .016 | 5.50 | .021 | 14 |
| 8 | 70 | .185 | .025 | 5.56 | .020 | 17 |
| 10 | 87 | .176 | .028 | 5.65 | .021 | 33 |
| 12 | 104 | .177 | .033 | 5.74 | .023 | 17 |
| 14 | 122 | .170 | .037 | 5.97 | .021 | 49 |

The results here suggest that a transfer function fit would remain the same out to the maximum airspeed of interest with nearly the same pendulum frequency and small negative damping ratios, so that a controller designed from the available models will remain effective at the higher speeds. This turns out to be the case as is shown from the closed-loop tests described later in this paper.

## PRELIMINARY DESIGN OF ACH CONTROLLER

**Design Considerations**

The preliminary design of the ACH controller for the M119 slung load applied classical control design methodology. The design used longitudinal and lateral cable angle feedback to damp longitudinal and lateral load pendulum motion by translation of the active cargo hook. The preliminary design was based on hand-tuning of the controller gains and frequencies. The design was then optimized as described in the next section. As described above, the ACH controller is a direct control mechanism that automatically adjusts the hook position to improve load damping and system stability without pilot command. The idea of using onboard active actuator control was examined in the past research for hover and low speed flight (Refs. 14 and 15). The current paper focuses primarily on controller performance during high speed flight where the potential for load instability exists.

As indicated above, the slung load pendulum dynamics were obtained as linear models identified from open loop frequency sweep tests in the wind tunnel. Test results showed that the cable angle response to ACH translation correlated highly with on-axis responses ($\theta_c/x, \phi_c/y$) and off-axis responses were negligible. The linear model parameters ($K, \zeta_p, \omega_P, \tau$) were scheduled by airspeed due to dependence of system dynamics on dynamic pressure.

Figure 9 shows a model of the open loop system with the active cargo hook and external slung load. The active cargo hook is modeled as a first order actuator with a bandwidth of 20 rad/s determined by the time constant ($\tau_a$). A time delay was included in the slung load dynamic model to represent actuator command and sensor delays. The time delay was neglected during the design process, but was later included to analyze closed-loop stability.

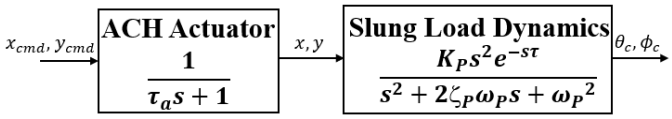


**Figure 9. Model of the open loop system with active cargo hook and external slung load.**

The open loop transfer functions can be converted into two sets of equations of motion representing the longitudinal and lateral axes of the load pendulum motion as shown in Equations (2)-(3).

$$\ddot{\theta}_c + 2\zeta_P \omega_P \dot{\theta}_c + \omega_P{}^2 \theta_c = K_P \ddot{x} \quad (2)$$

$$\tau_a \cdot \dot{x} + x = x_{cmd}(t - \tau) \quad (2.1)$$

$$\ddot{\phi}_c + 2\zeta_P \omega_P \dot{\phi}_c + \omega_P{}^2 \phi_c = K_P \ddot{y} \quad (3)$$

$$\tau_a \cdot \dot{y} + y = y_{cmd}(t - \tau) \quad (3.1)$$

It can be seen that cable angle motion is related to the acceleration of the cargo hook ($\ddot{x}, \ddot{y}$) for each axis. Tables 2 and 3 show that the damping of the load pendulum motion increases with airspeed, especially for the lateral axis. As indicated earlier, at high airspeeds (greater than 122 kts and 174 kts full scale depending on model and axis), valid linear models could not be identified due to unstable oscillatory motion of the load. It was expected that such unstable behavior would be stabilized by controllers designed using data from stable linear models.

## Controller Design

*Design for Hover Condition*

The load at the hover condition was selected to demonstrate the controller design approach since it had the smallest damping ratio of all airspeeds. The firing configuration was selected as the primary configuration for controller design. However, the pendulum dynamics for the firing and folded configurations were similar as shown in Tables 2 and 3. The lateral axis controller design was considered prior to the longitudinal axis. Figure 10 shows the step response of the open loop system at hover for the firing configuration and lateral axis, which demonstrates the low damping of the pendulum mode without any compensation.

*The Use of Filters and Compensators*

Previous investigations of helicopter external slung load showed that dynamic compensation was effective in increasing system stability and reducing swinging motion of the load at low airspeed (Refs. 14, 24). Thus, the use of dynamic compensation was considered for the ACH controller design. The block diagram in Figure 11 shows the model of the closed-loop system.

Lead and lag compensation were both considered for the controller design. Controller filter, compensator, and gain parameter values are listed in Table 4.

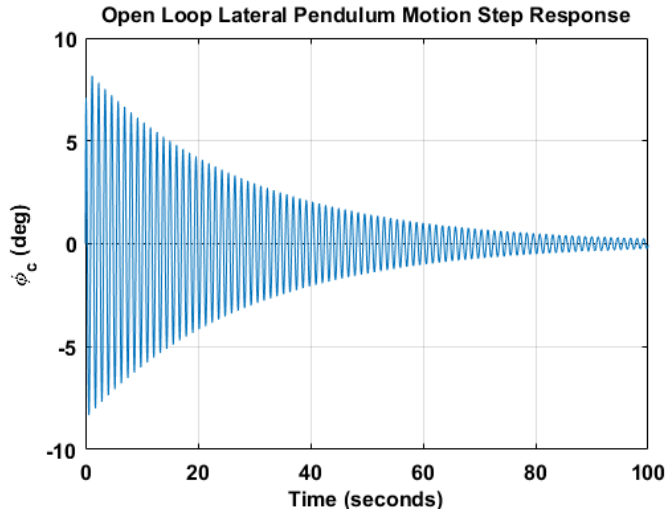


**Figure 10. Open loop simulation of lateral pendulum motion step response, (hover, firing configuration).**

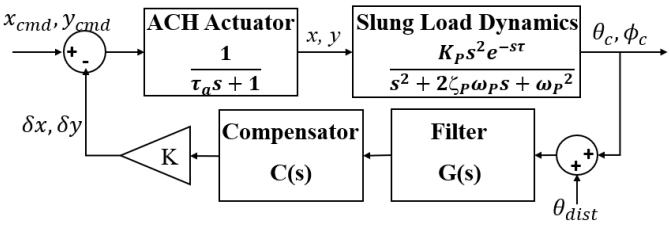


**Figure 11. Block diagram of the closed-loop system.**

**Table 4. Controller parameters for lateral pendulum mode, (hover, firing configuration).**

| | Filter G(s) | Compensator C(s) | Gain K |
|---|---|---|---|
| Lead Design | $1/(s+p)$ $p = 7.04, \frac{rad}{s}$ | $s$ | $-4.12, \frac{mm}{deg}$ |
| Lag Design | $s/(s+p)$ $p = 0.1, \frac{rad}{s}$ | $1/(s+d)$ $d = 1.85, \frac{rad}{s}$ | $28.6, \frac{mm}{deg}$ |

*Lead Design at Hover*

Using proportional derivative (PD) feedback has the benefit of improving system damping and providing a quicker transient response. For the lead design, the controller transfer function was composed by combining a pure derivative term ($\boldsymbol{s}$) and low pass filter ($\frac{1}{s+p}$), which was used to decrease controller response to high frequency disturbances to cable angle. The parameters of the lead design are listed in Table 4. The lead design used a negative gain value that shifted the phase of the output of the controller by 180 deg. so that the cargo hook motion was opposite in sign to the lateral cable angular rate.

Lead compensator parameters were obtained by manual tuning using the control system toolbox in MATLAB™. Design started by placing system zeros at the origin and the pole of the lag filter at the pendulum natural frequency. The lead was gradually adjusted until the shape of the pole trajectories became stable and well-damped. The compensation induced phase lead at the resonance of the swinging load by driving the cargo hook to move in lead of the load response. Figure 12 shows the root locus plot of the closed-loop system with the lead design. The closed-loop pole trajectories of the pendulum mode shifted toward the left of the s-plane, thus improving system stability and damping. However, the closed-loop system now had an extra set of poles due to the mixing of actuator and the low pass filter that could shift to the unstable region when the gain was high. The broken loop response in Figure 13 shows two sets of phase margins occurring at two different gain crossover frequencies. The smallest between the two would be selected as the minimum margin. The delay margin indicated the tolerance of the system toward time delay and was calculated based off the phase margin (PM) and the crossover frequency ($\omega_{gc}$) of the closed-loop system as shown in Equation 4.

$$DM = \frac{PM}{\omega_{gc}} * \frac{\pi}{180^\circ} \text{ (s)} \quad (4)$$

For a phase margin of 22.4 deg. at 7.71 rad/s, the resulting delay margin (DM) of 0.0506s just barely surpassed the measured time delay (0.0246s). Additional time delay has a destabilizing effect on the control system and decreases the effective damping of the controller. Therefore, higher delay margin represents good system robustness toward change of delay factors during operation.

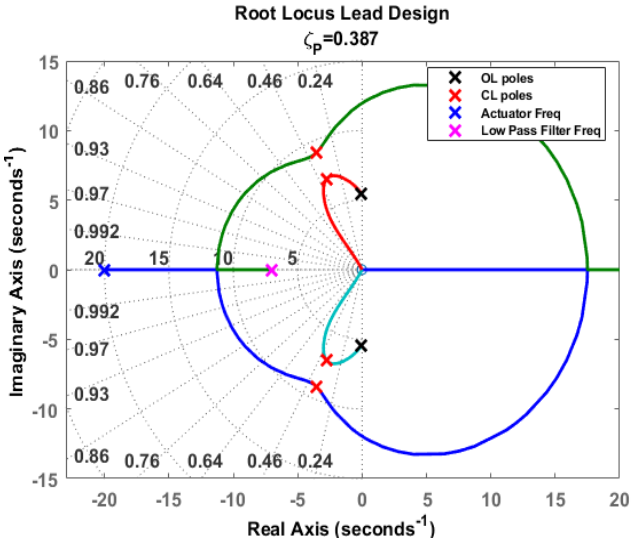


**Figure 12. Root locus plot of lateral pendulum mode with lead compensation, (hover, firing configuration).**

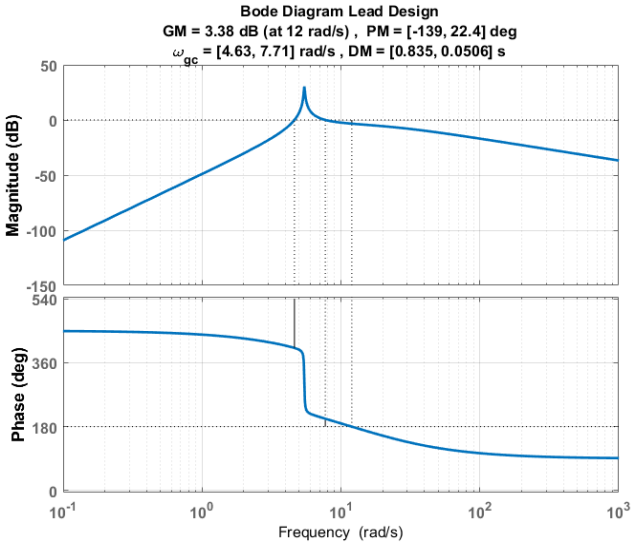


**Figure 13. Broken-loop Bode diagram of lateral pendulum mode with lead compensation, (hover, firing configuration).**

Figure 14 shows the simulated closed-loop step response of the load lateral pendulum motion with lead compensation. Compared with the open loop step response, there is a significant decrease in the time required for the lateral cable angle to settle back to the zero position, and the oscillation of the lateral angle is damped quickly, despite an increase in overshoot during the initial transient response. The second plot shows the lateral control command to the ACH actuator $\delta y$. The control signal moves in opposite sign with the lateral cable angle and has a lead tendency. The time history plot shows that the lead design improved the damping of the lateral pendulum mode. However, as shown by the Bode plot, small stability margins reflect weak robustness, which imposes higher risk of the system becoming unstable due to changes in load and control system parameters.

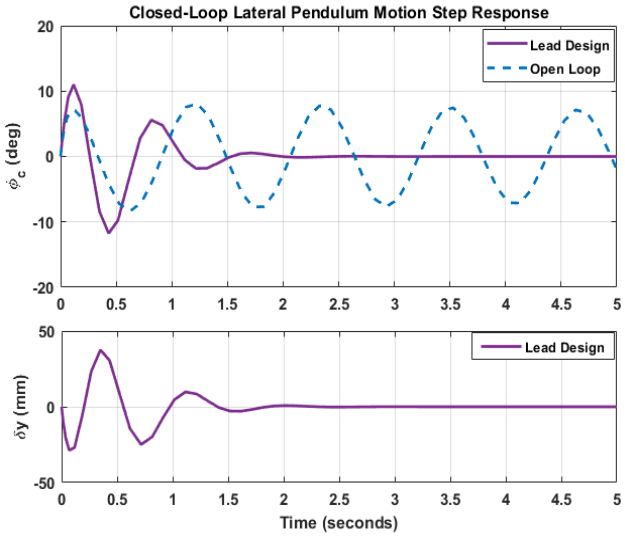


**Figure 14. Closed-loop simulation of lateral pendulum motion step response with lead compensation, (hover, firing configuration).**

*Lag Design at Hover*

Another approach for slung load control is to use lagged cable angle feedback. In Ref. 16, it was shown in simulation that a compensator with a lag filter could be tuned to achieve proper phasing between load swing and control input to dampen the swing motion at hover and low speed flight. The approach was modified for application to the ACH controller. A washout filter ($\frac{s}{s+p}$) was used to remove actuator response to steady state trailing cable angles, which occur during a change in flight speeds. The lag compensator ($\frac{1}{s+d}$) created additional phase lag in the system over the inherent phase delay from the actuator and also provided filtering of high frequency signals from the sensor. This control structure was demonstrated in flight on an H-6 helicopter by Boeing and the U.S. Army Aeroflightdynamics Directorate (Ref. 19). The parameters of the controller are listed in Table 4 for the selected hover case. The washout filter frequency was chosen to be very small to reject steady state trailing cable angles, and the lag compensator frequency was manually tuned to achieve the proper phasing.

The root locus plot for the lag design (Figure 15) shows better damping compared to the lead design and all the closed-loop trajectories are in the stable region. The broken-loop

response (Figure 16) shows significant increases in gain margin and phase margin as compared to the lead design. The minimum delay margin of 0.1755 s also increased significantly and was well above the measured time delay of the identified linear model (0.0246 s). The negative phase margin indicated a stable system since it was measured from the +180° line. The higher damping ratio achieved by the lag design is reflected by the time history plot comparison (Figure 17) of the simulated closed-loop system for the two controllers. The lateral cable angle response shows smaller amplitude of the oscillation and shorter settling time compared with the lead design. The actuator usage is also significantly reduced for the lag design as shown in the second plot. Therefore, the lag compensation has better performance in terms of system damping and stability than the lead design at hover for the firing configuration.

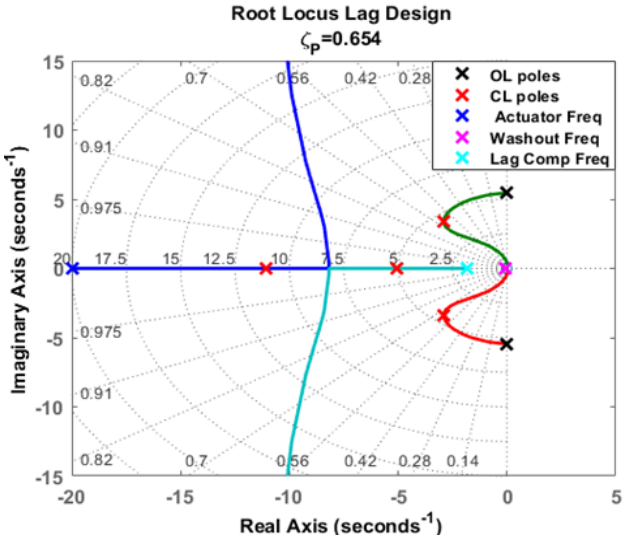


**Figure 15. Root locus plot of lateral pendulum mode with lag compensation, (hover, firing configuration).**

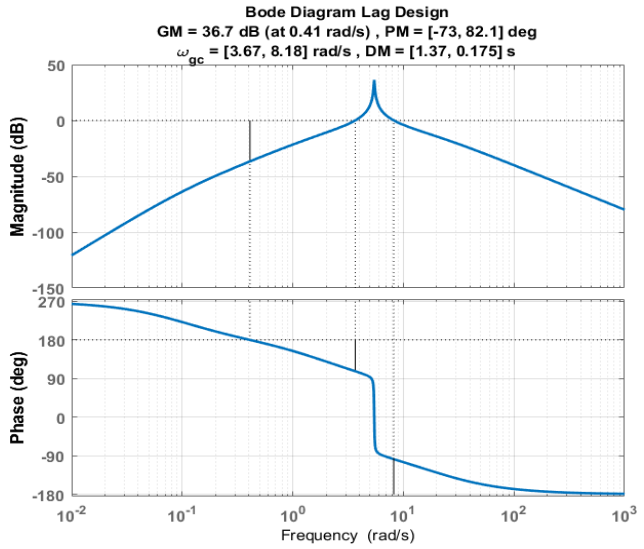


**Figure 16. Broken-loop Bode diagram of lateral pendulum mode with lag compensation, (hover, firing configuration)**

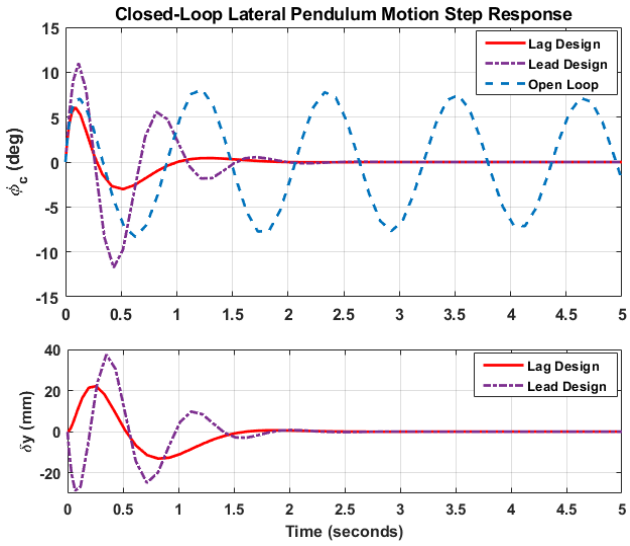


**Figure 17. Closed-loop simulation of lateral pendulum motion step response with lag compensation, (hover, firing configuration).**

*Design for Forward Flight*

Lag compensation was shown to improve the damping of the load motion for the hover condition for the firing configuration and lateral axis. The next design objective was to tune controller parameters for forward flight conditions and analyze controller performance. During the design process, it was discovered that controller performance was not very sensitive to increases in airspeed. For the controlled system, the damping of the pendulum modes varied over a range of 0.5-0.8 with a trade-off between overshoot and settling time. The gain values for other conditions also required relatively small adjustments for maximum damping. Therefore, the controller designed for the hover condition was tested for forward flight conditions and the responses were found to show only small sensitivity to airspeed.

Figure 18 shows the time history of the lateral cable angle at various airspeeds subjected to the same step input as the hover condition. The three non-zero airspeeds, corresponding to 52, 87 and 122 kts FS, agree closely with the hover case using the same controller. Therefore, the compensation proved to be effective throughout the flight envelope where the linear models were available.

*Controller Validation for the Longitudinal Axis and the Folded Configuration.*

Lag compensation was proven to be effective in increasing damping and stability of the load lateral pendulum motion in both hover and forward flight. As previously mentioned, firing and folded configuration pendulum dynamics were very similar as shown in Tables 2, 3. Additionally, the pendulum dynamics were similar for the longitudinal and lateral axes in both configurations. For the longitudinal axis at all airspeeds, the closed-loop system had a damping ratio above 0.5. This implied that a universal controller could work for both axes across all airspeeds.

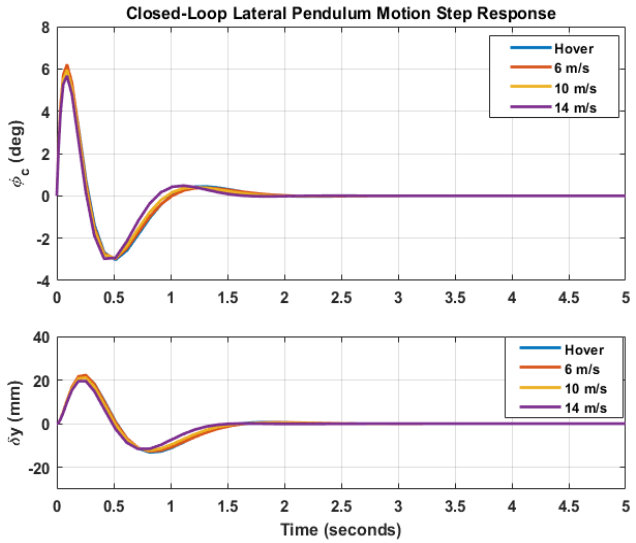


**Figure 18. Closed-loop simulation of lateral pendulum motion step response with lag compensation, (multiple airspeeds, firing configuration).**

The controller gain for the folded configuration was slightly adjusted to achieve maximum damping for the hover case and the controller performance was verified in other airspeeds. Table 5 lists the airspeed independent controller parameters for the firing and folded configurations and the lateral and longitudinal axes. Note that the gain value K for the folded configuration was later modified during the controller optimization. The value listed in Table 5 was designed for the hover condition for maximum damping in both lateral and longitudinal axes. During the optimization process, a different controller gain was used as a starting value for controller tuning.

**Table 5. Preliminary ACH controller parameters.**

| Parameter | Firing (Lon) | Firing (Lat) | Folded (Lon) | Folded (Lat) |
|---|---|---|---|---|
| K (gain) (mm/deg) | -28.6 | 28.6 | -29.0 | 29.0 |
| d (lag) (rad/sec) | 1.85 | 1.85 | 1.85 | 1.85 |
| p (washout) (rad/sec) | 0.10 | 0.10 | 0.10 | 0.10 |

Tables 6, 7 list the system stability margins for two wind tunnel speeds (corresponding to 52 and 122kts FS) with the lag compensation. They show that the proposed controller can provide good damping and stability to the external slung load in both configurations under different airspeeds without gain scheduling.

The last step of the design was to verify the robustness of the system to time delay uncertainty. The measured time delays of various linear models were all below 0.025 s with the largest being 0.0246 s at hover. The system was simulated in Simulink™ with an integrated transport delay block acting as the delay factor. Figure 19 shows the step response of the closed-loop system at hover for the firing configuration. The orange line represents the lateral response of the load with a time delay equal to the delay margin (0.175 s). The response was highly oscillatory, which was caused by the decrease of effective damping of the control system due to the presence of time delay. The delay factor was slowly increased until the system became unstable (shown in blue line), which happened at $\tau$ = 0.181 s. This confirmed that the tolerance of the system toward time delay was around the calculated delay margin by a small deviation. The purple line represents the system with the actual time delay from the linear model and the result shows that the damping and stability of the system were not affected by such time delay, which assures good robustness of the control system during operation.

**Table 6. System stability margins in firing configuration.**

| Firing Config. | Axis | GM (dB) | PM (deg) | DM (sec) |
|---|---|---|---|---|
| 6 m/s | $\theta_c/x_{cmd}$ | 38.1 | -78.3 | 0.186 |
| | $\phi_c/y_{cmd}$ | 36.6 | -74.3 | 0.173 |
| 14 m/s | $\theta_c/x_{cmd}$ | 39.7 | -88.0 | 0.187 |
| | $\phi_c/y_{cmd}$ | 38.7 | -82.5 | 0.175 |

**Table 7. System stability margins in folded configuration.**

| Folded Config. | Axis | GM (dB) | PM (deg) | DM (sec) |
|---|---|---|---|---|
| 6 m/s | $\theta_c/x_{cmd}$ | 36.4 | -74.1 | 0.175 |
| | $\phi_c/y_{cmd}$ | 36.2 | -74.0 | 0.164 |
| 14 m/s | $\theta_c/x_{cmd}$ | 36.1 | -75.1 | 0.193 |
| | $\phi_c/y_{cmd}$ | 36.8 | -80.4 | 0.147 |

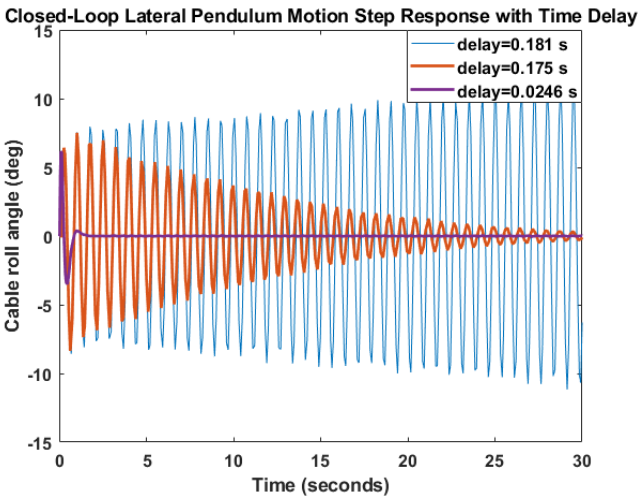


**Figure 19. Closed-loop simulation of lateral pendulum motion step response with time delay, (hover, firing configuration).**

## OPTIMIZATION OF ACH LAG CONTROLLER

Using the same lagged cable angle feedback plus washout controller architecture as the preliminary design, the controller design parameters *K* (gain), *d* (lag), and *p* (washout) were optimized using CONDUIT®, a flight control design and optimization software (Ref. 25). CONDUIT® uses a specification-driven optimization approach that enforces all performance requirements with minimum actuator usage. For use in CONDUIT®, the closed loop system was implemented in a Simulink model containing the controller architecture, slung load dynamics, and active cargo hook actuator dynamics with rate and position limits as shown in Figure 20. Additional details on the definition of optimization objectives and the CONDUIT® control system design process can be found in (Ref. 25). The design point for the optimization is 10 m/s (87kts FS).

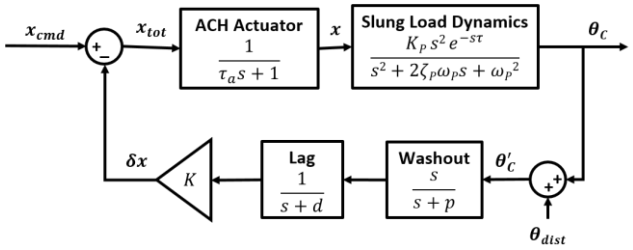


**Figure 20. Linearized simulation model with controller architecture used for control system design and optimization in CONDUIT®. Model includes longitudinal and lateral axis actuator rate and position limits of ±100 mm/s and ±100 mm, respectively**.

Many standard CONDUIT® specifications (eigenvalues, robust stability, gain and phase margins, damping, actuator RMS, minimum and maximum crossover, and actuator rate limiting) were used for optimization. Additionally, four time domain specifications were developed to characterize linear and nonlinear motion of the hook and sling in response to disturbances in cable angle:

1. *10% settling time of actuator position for 45 deg 1–cosine cable angle gust:* Ensures the actuator re-centers in *less than 15 sec* in response to a large gust disturbance. Use of 1-cosine gusts for evaluation of controller disturbance rejection performance is described in Ref. 25.
2. *Max peak-to-peak cable angle for 45 deg 1–cosine cable angle gust*: Ensures load motion *less than 5 deg* peak-to-peak in response to a large gust disturbance.
3. *Max magnitude of actuator position for 5 deg 1–cosine cable angle gust*: Ensures actuator position magnitude *less than 30 mm* in response to a small gust disturbance.
4. *10% settling time of actuator position for 1 deg/s ramp cable angle disturbance:* Ensures the actuator re-centers in *less than 75 sec* in response to a ramp-and-hold disturbance to cable angle. The input is a 1 deg/s ramp to 45 deg, then is held at 45 deg. This input mimics the systematic trail angle behavior in a typical acceleration from hover to the maximum operational speed.

The quantitative values set as requirements for settling time, peak-to-peak, and magnitude for these four specifications were selected to improve controller performance and actuator usage from that of the preliminary controller design. Three of the four specifications set requirements for actuator position responses since actuator position limits were important to consider due to the space constraints of the HIL wind tunnel setup and when implementing on a full-scale aircraft.

Additionally, the complete set of frequency and time domain specifications ensures that the optimization problem is well-posed; that is, that each of the three design parameters is sensitive to at least one of the specifications. In particular, the washout parameter, *p*, was sensitive to the 10% actuator settling time specification for the ramp-and-hold disturbance. The washout ensures re-centering of the hook in the presence of steady cable angles such as occurs with the trail angle in forward flight or the lateral cable angle during steady turns. The gain, *K*, and lag parameter, *d*, were more sensitive to other specifications such as damping.

Figure 21 shows the optimized controller results for each specification as they appear in CONDUIT® for the firing configuration, longitudinal axis, at 10 m/s as an example. The optimized design achieves the desired, or Level 1, performance (blue region) for all specifications. Table 8 summarizes the Level 1 requirements for the specifications and the corresponding performance achieved by the preliminary (pink symbols) and optimized (yellow symbols) control system designs. Figure 22 overlays the four key time domain responses for the preliminary and optimized designs for the firing configuration, longitudinal axis, at 10 m/s.

The results in Table 8 demonstrate that the preliminary and optimized controller designs provide ample stability margin above the 6 dB, 45 deg requirement. The two designs have damping ratios of 0.65 and 0.35, respectively, which meet the requirement of 0.35 and significantly improve on the value of 0.03 identified for the open loop system and listed in Table 3. Comparison of the four time domain specification results listed in Table 8 and plotted in Figure 22 indicate key trade-offs between the two controller designs in the time domain:

1. The results for *10% settling time of actuator position [s] for 45 deg 1–cosine cable angle gust* demonstrate that the optimized design re-centers 39% more quickly in response to a large gust disturbance.
2. The results for *max peak-to-peak cable angle [deg] for 45 deg 1–cosine cable angle gust* demonstrate that the preliminary design improves reduction of load motion by 18% in response to a large gust.
3. The results for *max magnitude of actuator position [mm] for 5 deg 1–cosine cable angle gust* demonstrate that the optimized design has 37% more efficient use of the actuators as measured by maximum magnitude of actuator position in response to a small gust.
4. The results for *10% settling time of actuator position for 1 deg/s ramp disturbance* demonstrate that the preliminary design re-centers 7% more quickly after a ramp disturbance, which is equivalent to a change in flight speeds.

Thus, the results above also indicate a key trade-off for the two controller designs between damping and actuator usage as measured by maximum magnitude of actuator position in response to a 5 deg 1-cosine cable angle gust. While the preliminary design has higher damping than the optimized design (0.65 and 0.35, respectively), this comes at the expense of increased actuator usage (magnitudes of 36.06 mm and 22.84 mm, respectively). This trade-off between controller performance and actuator usage has important implications since space constraints may limit actuator throw when implementing an active cargo hook on a full-scale aircraft. Examination of design parameters indicates that this trade-off is primarily due to the higher gain, *K*, of the preliminary design, which is the primary difference between the two controllers design. .

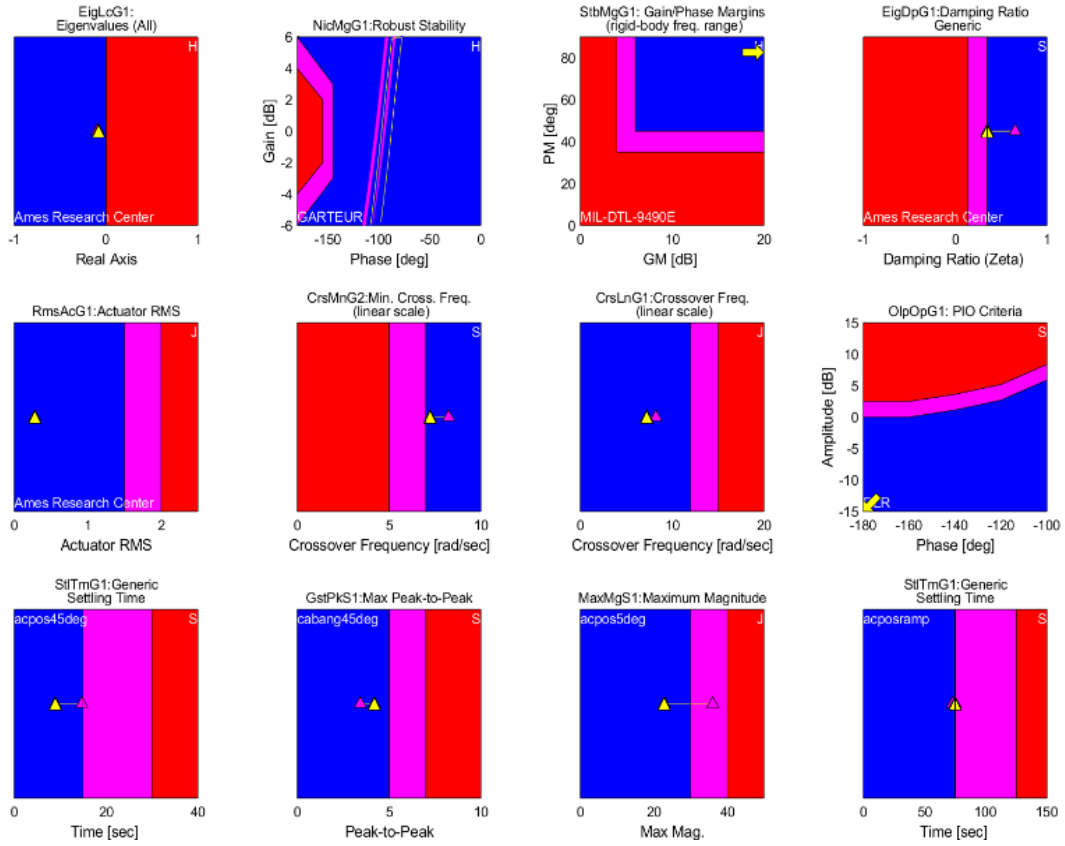


**Figure 21. Optimized design (yellow symbols) and preliminary design (pink symbols) controller performance for the firing configuration, longitudinal axis, at 10 m/s.**

**Table 8. Controller Performance Metrics (Firing, Longitudinal, 10 m/s)**

| Specification | Description | Level 1 Requirement | Preliminary Design | Optimized Design |
|---|---|---|---|---|
| EigLcG1 | Eigenvalues | All Left-Hand Plane | All Left-Hand Plane | All Left-Hand Plane |
| NicMgG1 | Robust Stability | See Fig. 21 | Level 1 | Level 1 |
| StbMgG1 | Stability Margins | [6.0 dB, 45.0 deg] | [37.5 dB, 77.7 deg] | [42.9 dB, 82.6 deg] |
| EigDpG1 | Damping | 0.35 | 0.65 | 0.35 |
| RmsAcG1 | Normalized Actuator RMS | 1.50 | 0.28 | 0.28 |
| CrsMnG2 | Min Crossover | 7.0 rad/s | 8.2 rad/s | 7.2 rad/s |
| CrsLnG1 | Max Crossover | 12.0 rad/s | 8.2 rad/s | 7.2 rad/s |
| OlpOpG1 | Actuator Rate Limiting | See Fig. 21 | [-204.1 deg, -23.4 dB] | [-203.9 deg, -27.3 dB] |
| StlTmG1 (Gust) | Settling Time Actuator Position (45 deg Gust) | 15.00 s | 14.74 s | 8.96 s |
| GstPkS1 | Max Peak-to-Peak Cable Angle (45 deg Gust) | 5.00 deg | 3.44 deg | 4.20 deg |
| MaxMgS1 | Max Magnitude Actuator Position (5 deg Gust) | 30.00 mm | 36.06 mm | 22.84 mm |
| StlTmG1 (Ramp) | Settling Time Actuator Position (Ramp) | 30.00 s (after ramp) | 27.87 s (after ramp) | 30.00 s (after ramp) |

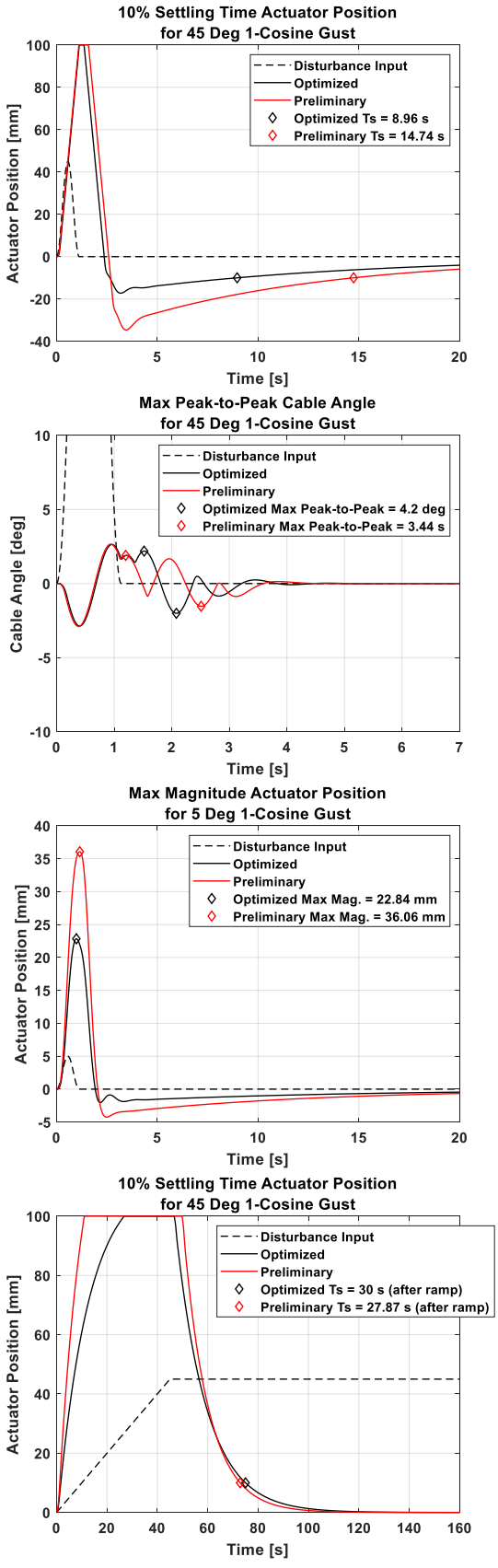


**Figure 22. Comparison of key time domain responses for the optimized and preliminary controller designs for the firing configuration, longitudinal axis, at 10 m/s.**

Table 9 shows the preliminary and optimized designs for the firing and folded configurations, longitudinal and lateral axes, at a wind tunnel speed of 10 m/s. The control system design parameters were designed for the lateral axis and, due to the similar dynamics of both axes as determined from open loop system identification, the longitudinal axis parameters were constrained to have the same magnitudes.

**Table 9. Preliminary and Optimized Controller Designs (Firing/Folded Configurations, Longitudinal/Lateral Axes, 10 m/s)**

| Design | Parameter | Firing (Lon) | Firing (Lat) | Folded (Lon) | Folded (Lat) |
|---|---|---|---|---|---|
| Preliminary | K (gain) | -28.60 | 28.60 | -24.20 | 24.20 |
| | d (lag) | 1.85 | 1.85 | 1.85 | 1.85 |
| | p (washout) | 0.10 | 0.10 | 0.10 | 0.10 |
| Optimized | K (gain) | -18.67 | 18.67 | -19.02 | 19.02 |
| | d (lag) | 2.02 | 2.02 | 1.92 | 1.92 |
| | p (washout) | 0.08 | 0.08 | 0.08 | 0.08 |

## CLOSED LOOP TESTS

The two controllers that were described above (preliminary and optimized) were implemented into the computer of the HIL wind tunnel test setup. The real time measured cable angles were fed into a code that calculated the required motion of the hook. Both controllers were able to stabilize the slung loads through the entire flight speed envelope.

Figure 23 shows the model attitude angles (pitch, roll, and yaw), cable angles, , and the ratio between the cable force and load weight, of the folded configuration during a relatively slow increase of the tunnel speed over a range corresponding to 87kts FS up to 190 kts FS. The controller in this case is the preliminary one. The behavior of the "steady state" values is similar to their behavior during the open loop test that is shown in Figure 3. The ability of the controller to suppress the LCO of the model and cable angles is clearly shown. When the optimized controller is used the behavior is very similar.

Figure 24 shows the behavior of the firing configuration during a relatively slow increase of the tunnel speed over a range corresponding to 87kts up to almost 165 kts FS, when the longitudinal trail angle exceeds 42 deg. In this case the optimized controller is used. When compared with the results of Figure 5 for the open loop test, the capability of the controller to suppress the severe instability above 130 kts FS is evident. Also in this case the behavior is very similar when the preliminary controller is applied.

The simulation results for key responses obtained in CONDUIT® were validated by hardware-in-the-loop (HIL) dynamic wind tunnel testing. A test plan was developed with appropriate inputs and outputs to obtain the responses during testing. Figure 25 shows the list of tests used for simulation validation on the left, and representative input signal profiles on the right. The actuator rate and position limits in the simulation model were revised from the values in Figure 20 to agree more closely with the wind tunnel HIL system (Lon: ±160 mm/s, ±80 mm; Lat: ±160 mm/s, ±160 mm).

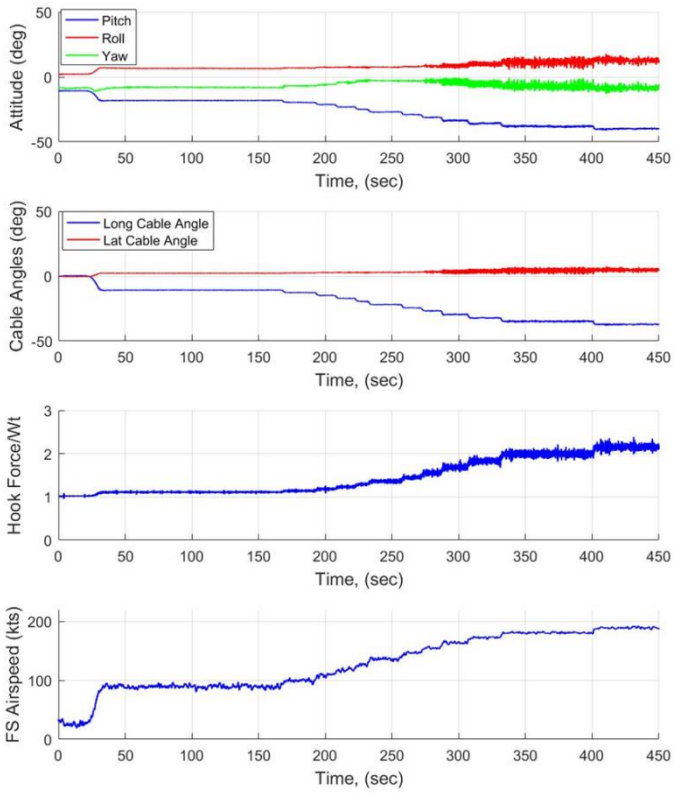


**Figure 23. The model attitude, cable angles, and ratio of hook force to weight, of the folded configuration during a slow increase of the tunnel speed when the preliminary controller is active.**

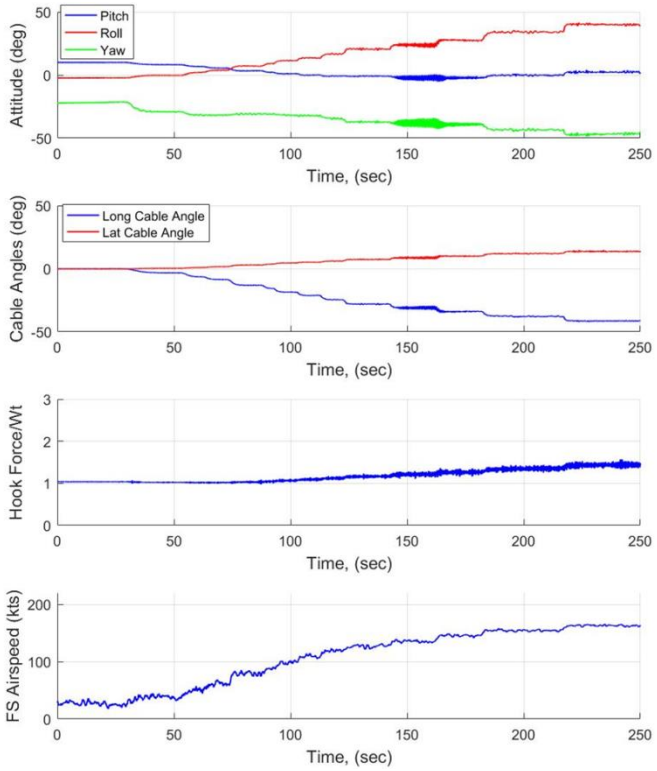


**Figure 24. The model attitude, cable angles, and ratio of the hook force to weight, of the firing configuration during a slow increase of the tunnel speed when the optimized controller is active.**

**Tests for Simulation Validation**

| Test | Test Name | Inputs | Outputs |
|---|---|---|---|
| 1 | 9 mm Frequency Sweep at Actuator Input | $x_{cmd}$ | $\theta_C$ $\delta x$ $x_{tot}$ |
| 2 | 3 mm Frequency Sweep at Disturbance Input | $\theta_{dist}$ | $\theta'_C$ |
| 3 | 45 deg (1 - Cosine) Disturbance | $\theta_{dist}$ | $\theta_C$ $x$ |
| 4 | 5 deg (1 - Cosine) Disturbance | $\theta_{dist}$ | $x$ |
| 5 | 1 deg/s Ramp Disturbance | $\theta_{dist}$ | $x$ |

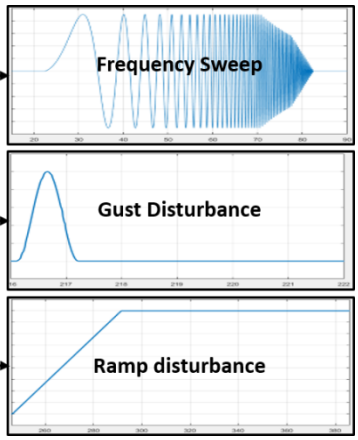


**Figure 25. Tests and associated inputs and outputs used for simulation validation in the wind tunnel.**

## ANALYSIS OF THE CLOSED LOOP RESULTS

### Simulation Validation

CIFER® was used to generate frequency responses from frequency sweeps of the CONDUIT® simulation model and the wind tunnel HIL system. Figures 26-29 overlay the closed and broken loop frequency responses generated from simulation and test data for the optimized controller for the folded and firing configurations, longitudinal and lateral axes, at 10 m/s (87 kts FS). The frequency responses show excellent agreement of simulation and test data over the frequency range with test data coherence greater than 0.6, which indicates that the input is linearly related to the output.

The frequency domain simulation validation was verified using the four time domain responses. Figure 30 overlays the key time domain responses generated from simulation and test data for the optimized controller for the folded/firing configurations, longitudinal/lateral axes, at 10 m/s. The time domain responses show good agreement of simulation and test

data. Similar good agreement was obtained for both controllers, both configurations, and both axes at 10 m/s.

These wind tunnel results validate the simulation model used for control system design and analysis in CONDUIT® for the M119 in the folded and firing configurations, longitudinal and lateral axes, at a wind tunnel speed of 10 m/s (87 kts FS).

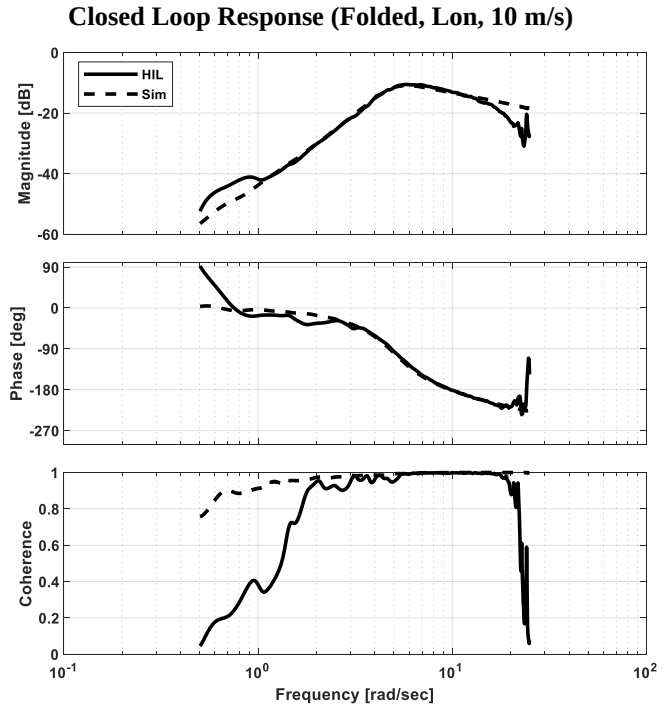


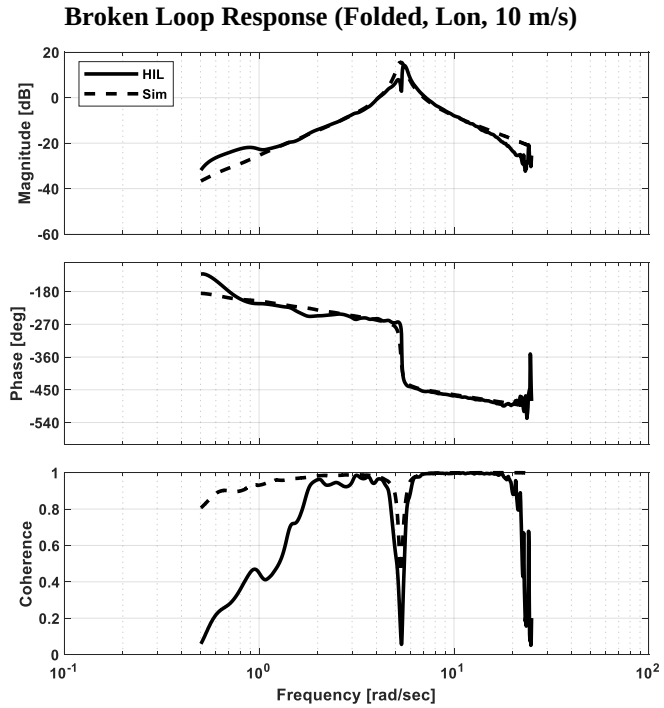


**Figure 26. Frequency domain simulation validations for the optimized controller for the folded configuration, longitudinal axis, at 10 m/s.**

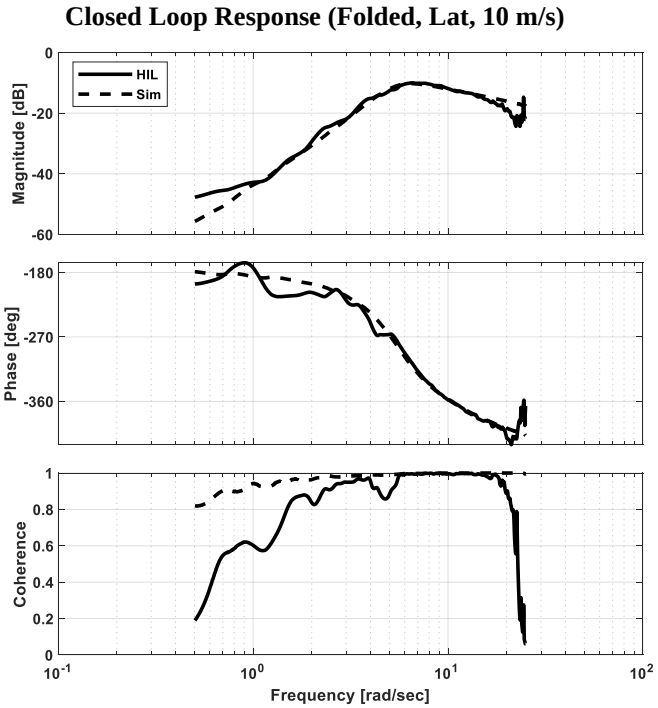


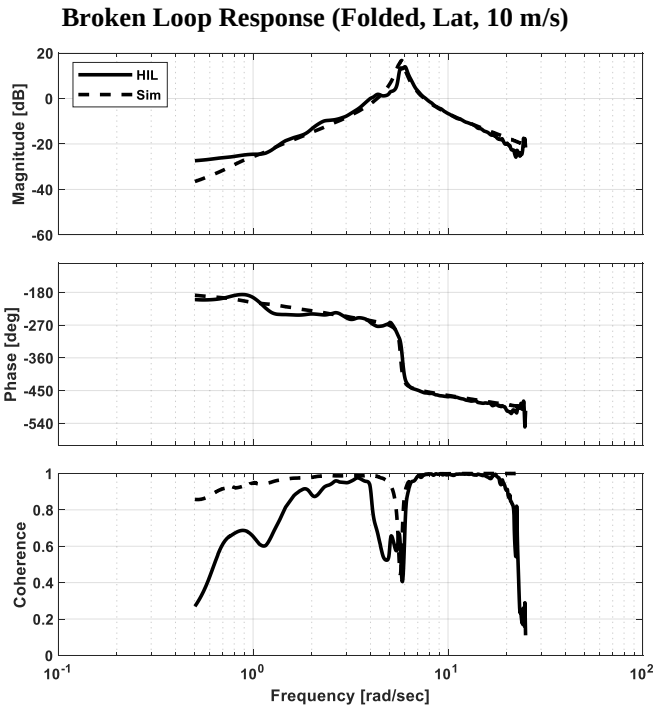


**Figure 27. Frequency domain simulation validations for the optimized controller for the folded configuration, lateral axis, at 10 m/s.**

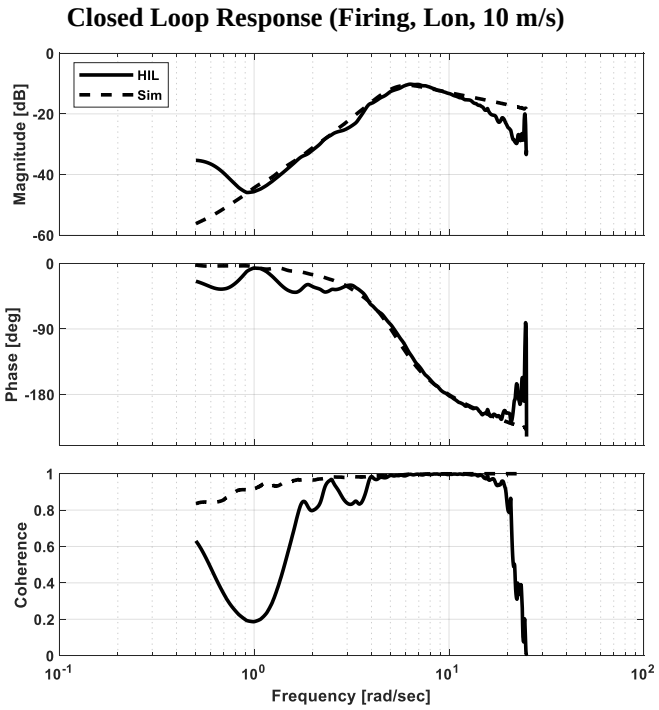


**Figure 28. Frequency domain simulation validations for the optimized controller for the firing configuration, longitudinal axis, at 10 m/s.**

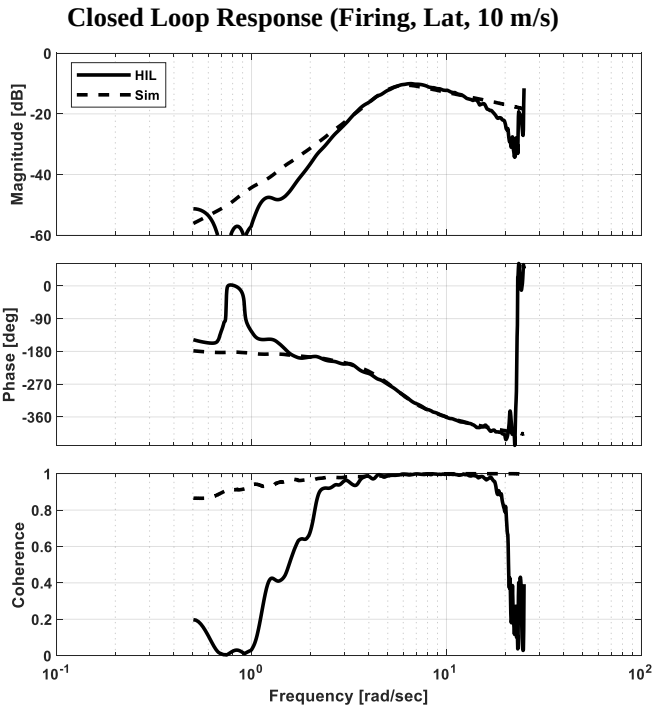


**Figure 29. Frequency domain simulation validations for the optimized controller for the firing configuration, lateral axes, at 10 m/s.**

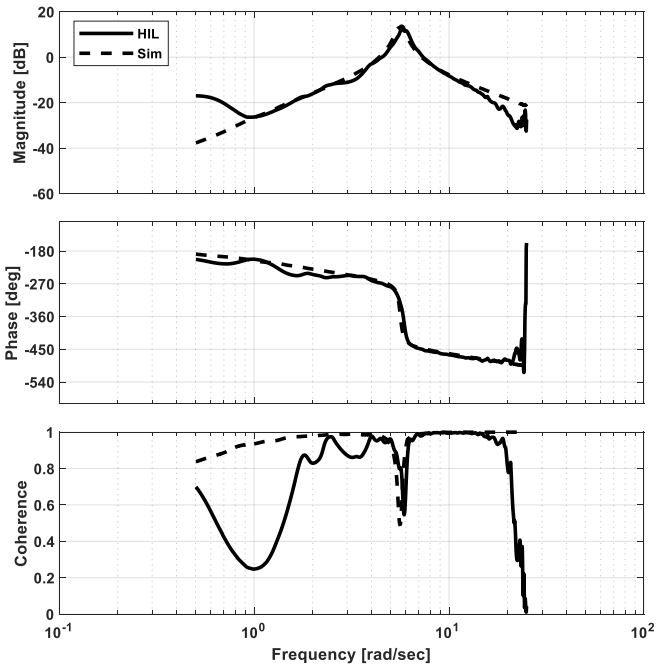


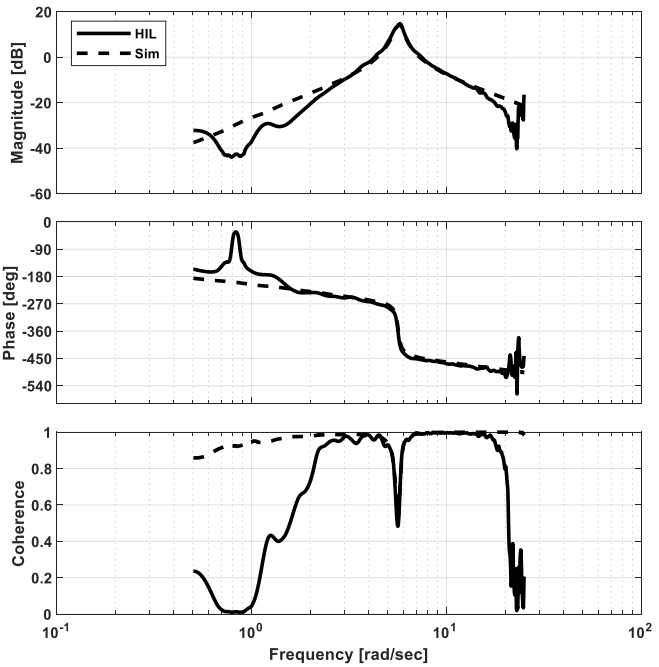

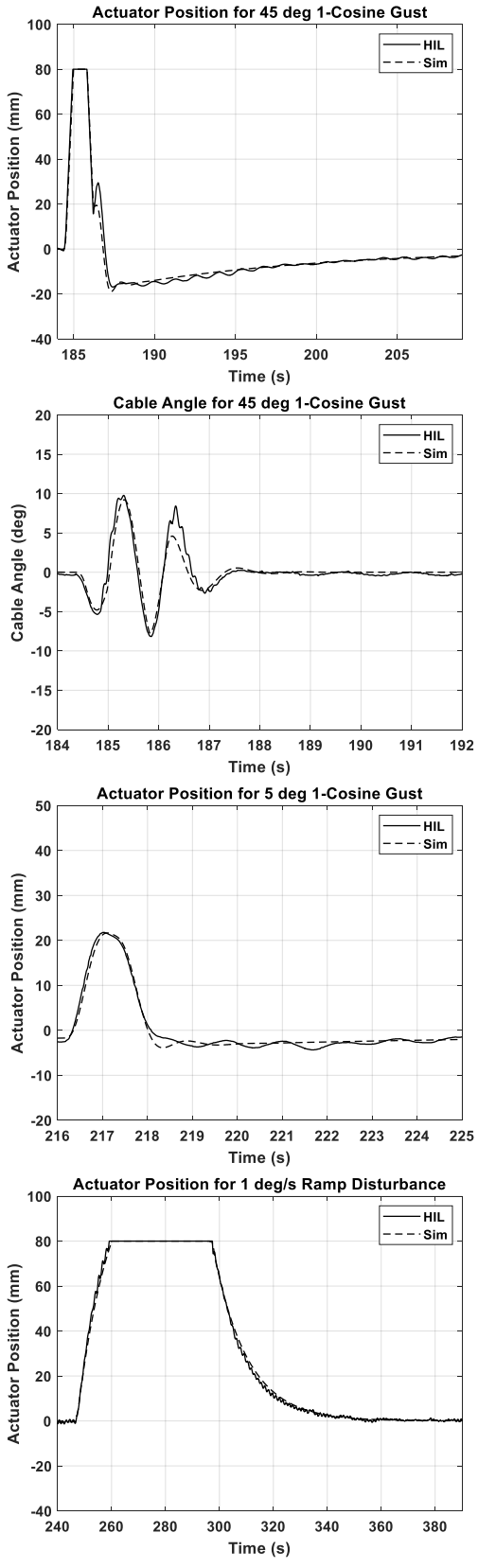


**Figure 30. Time domain simulation validation for the optimized controller for the folded configuration, longitudinal axis, at 10 m/s**

**Performance of the optimized controller at forward speeds**

The controller was tested at WT speeds above 10 m/s (87 kts FS) out to the limit of interest corresponding to the -45 deg trail angle operational safety limit. This was also the aft angular excursion limit of the tunnel setup that limited testing at the highest airspeeds of interest. The performance measures addressed here are (1) closed loop pendulum damping and (2) stability margins. The closed loop pendulum roots were obtained by fitting the pendulum transfer function to the closed loop frequency responses [$\theta c/x_{cmd}$] and [$\phi c/y_{cmd}$]. Example responses at 10 m/s are shown in Figures 26-29 and these exhibit the same magnitude peak and 180 deg. phase shift across the pendulum frequency previously seen in the open loop frequency response, except these features are not as sharply delineated in the closed loop response owing to the higher damping achieved by the controller. The stability margins are calculated from the broken loop frequency responses, [$\delta x/x_{tot}$], [$\delta y/y_{tot}$]. Example responses are shown in Figures 26-29.

Performance results for the optimized controller are given in Figures 31, 32 for the folded and firing configurations, respectively vs full scale airspeed. Values are obtained from the WT data at model scale. Damping, gain margin, and phase margin are the same at the equivalent full-scale airspeed, while the pendulum frequency scales down by $1/\sqrt{\text{scale}}$ from the values in the figures. For the folded configuration, pendulum damping is near or in the level 1 region ($\zeta \geq .35$) out to 191 kts FS. At the next higher test speed, 208.6 kts FS, the trail angle saturated the aft limit of the tunnel setup, precluding usable data. These results represent a significant improvement in damping compared to the very light damping of the uncontrolled dynamics given in tables 2 and 3 and this is extended to speeds where the uncontrolled dynamics are unstable. Although these tests did not include hover and low speeds, previous flight tests of the ACH in that speed regime showed that similar improvement in damping can be obtained from the ACH (Ref.17). Pendulum frequencies are approximately the same at all airspeeds and for both axes and unchanged from the open loop frequencies given in tables 2 and 3. The corresponding mean full-scale pendulum frequency is 1.25 rad/s. Gain margins are in the level 1 region (GM $\geq$ 6 dB), except at 174 kts FS where the lateral axis gain margin degrades slightly below level 1. There is a general trend of declining gain margin with airspeed. Phase margins are in the level 1 region (PM $\geq$ 45deg) at all test speeds.

For the firing configuration only three test speeds are available. Test speeds were limited by the aft cable angle limit of the tunnel setup. The results show that the ACH stabilizes the load with damping at the level 1 boundary. There are excess stability margins at the design speed (87 kts FS) but a rapid loss of gain and phase margin above that speed with some points below the level 1 boundary.

These results show that the ACH controller can extend the stable speed envelope of the M119 out to its highest usable speed corresponding to the operational limit on the trail angle (-45deg). While stability margins are reduced at speeds above

the design speed, it is expected that design adjustments and gain scheduling based on valid models of the higher speed dynamics will readily achieve the desired level 1 stability margins.

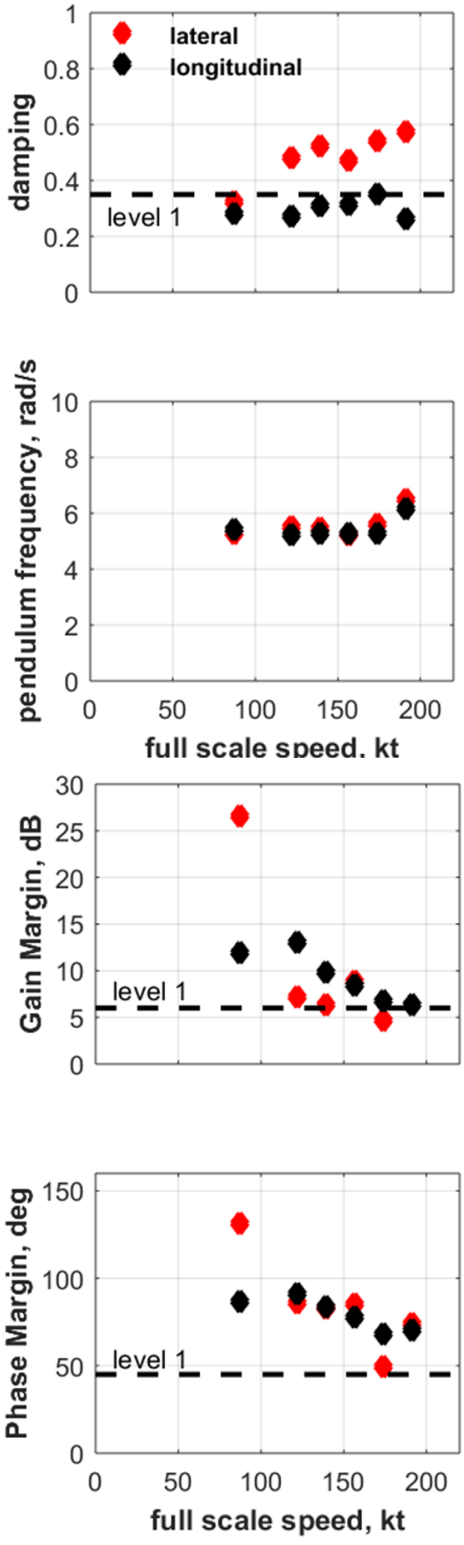


**Figure 31. Performance vs speed: folded configuration, optimized controller.**

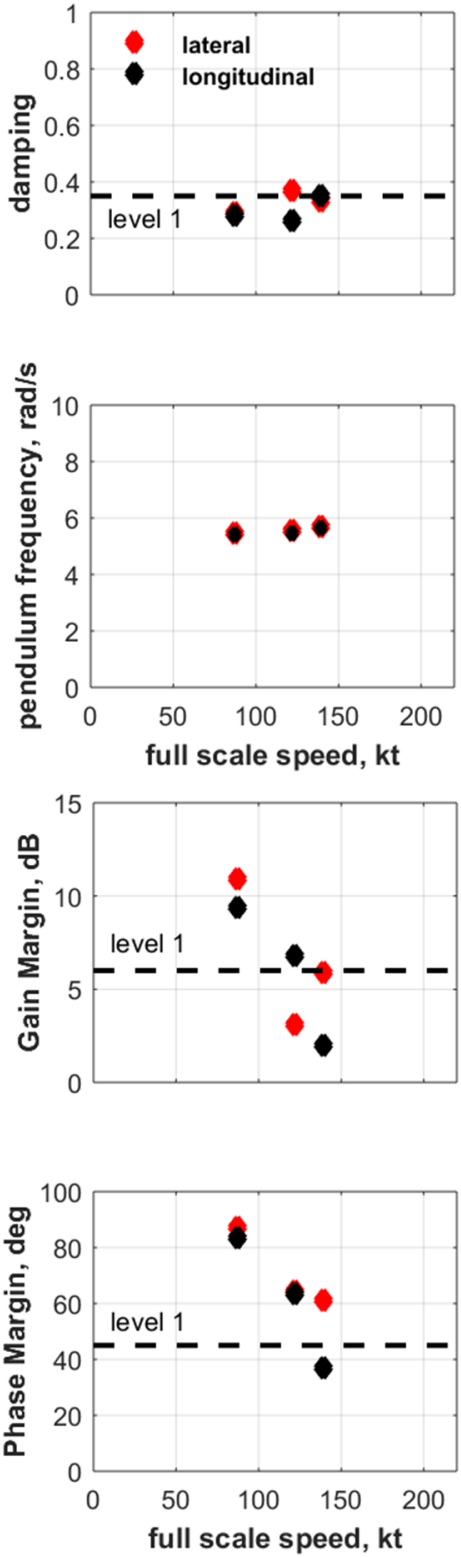


**Figure 32. Performance vs speed: Firing configuration, optimized controller.**

**Control Behavior during Maneuvering**

The washout removes the control offsets that would otherwise occur due to the steady state longitudinal cable angle in forward flight (trail angle). However, the controller responds to steady cable angle rates with steady offsets of the hook position, given from the controller transfer function in Figure 20 as (K/p*d)*$\Delta\dot{\theta}_c$, thus reducing the control margin available to regulate nonsystematic load motions and possibly saturating the control. Steady longitudinal cable angle rates occur for an extended period during steady accelerations or decelerations between hover and the maximum speed capability. In the event of extended position saturation, the controller is ineffective. Figure 33 shows a deceleration run in which wind tunnel speed is reduced in a sequence of ramp and hold stages and each ramp induces a corresponding trail angle ramp and excites the control, sometimes saturating the 80 mm actuator position limit. The wind tunnel speed deceleration in the test is about 0.1g (2 kts/s FS) which is within the deceleration limit for many helicopters used in slung load operations. It should be noted that the generous hook position and rate limits of the wind tunnel setup may not be available in a practical full scale ACH design. The effects of more severe limits remain to be addressed.

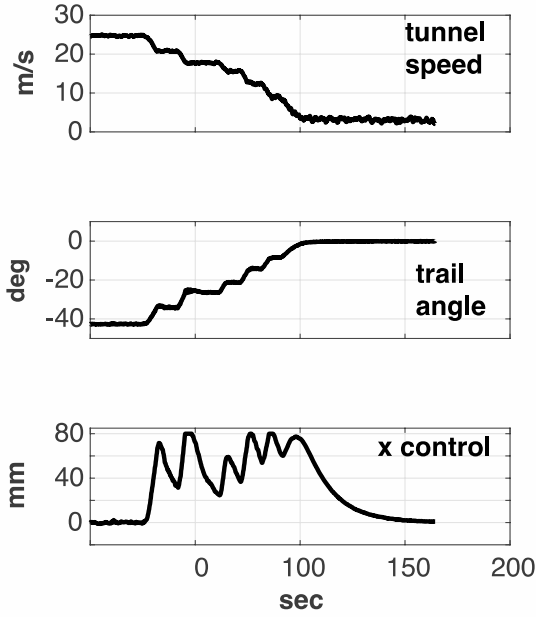


**Figure 33. Deceleration: folded configuration, optimized controller.**

## CONCLUSIONS

1. Previously, in cooperation with simulations and flight tests, wind tunnel tests proved to be a very useful tool for slung loads clearance and development of methods to stabilize problematic loads. In almost all the previous wind tunnel tests the hook location was fixed. The present investigation shows that using a wind tunnel hardware-in-the-loop (HIL) setup, where the hook can move and its movement is controlled in real time, improves further the advantages of wind tunnel tests. It was shown that HIL wind tunnel tests can be used to develop controllers for an active controlled hook (ACH) that suppress large LCO or severe instabilities that appear at high airspeeds. The controllers use the momentary cable angles as input for calculating the displacements commands to the hook.
2. The wind tunnel slung loads models in the present study were two configurations of the M119 Howitzer: folded and ready for firing. Tests showed that the two configurations adopt nearly steady cable angles and load yaw at low/medium speeds, but subject to large LCO or instabilities at high speeds.
3. Good linear models of the pendulum dynamics were obtained from wind tunnel data over the stable speed envelopes of the two configurations. The stable speed envelopes short of the 200 kts speed range of interest. The pendulum dynamics are nearly invariant with airspeed and very lightly damped at all stable airspeeds. It is likely, that the model will be the same at the unstable speeds, except with slightly negative damping.
4. The linear models were used for a preliminary design of the ACH controller. It was shown that the external load could be stabilized by using cable angle feedback with lag compensation in hover and forward flight conditions. The application of lag compensation, which was developed for hover and slow flight conditions, showed increased damping ratios and high stability margins at forward flight, along with satisfactory tolerance to time delay. The controller was integrated into the closed-loop system in each axis with universal parameters for all flight speeds, which suggests simplicity during implementation of the control structure into the wind-tunnel or flight tests.
5. Many standard CONDUIT® specifications were used for optimization of the ACH controller to enforce all performance requirements with minimum actuator usage. Additionally, four time-domain specifications were developed to characterize linear and nonlinear motion of the hook and sling. Results show that the preliminary and optimized controller designs provide ample stability margin and improve damping. There is an important trade-off between the controller designs in terms of damping and actuator usage.
6. The simulation used for the controller optimization has been validated in the frequency and time domains for both configurations, both controllers and both axes at the design speed of 87 kts using wind tunnel HIL test data.
7. Results from HIL tests at speeds above 10 m/s (87 kts FS) show that the ACH can stabilize the M119, in both carrying configurations, out to its maximum potential usable airspeed corresponding to the operational trail angle limit.
8. In the present investigation the HIL was used to develop and study an ACH to stabilize slung loads. The cable angles were the input data of the controllers. It will be interesting to further exploit the capabilities of the system. Thus for example, by running on the laptop a real time simulation of a helicopter that takes into account the hook force that is continuously measured, it will be possible to simulate the flight dynamics of the coupled helicopter/slung-load system.

## ACKNOWLEDGMENTS

This research was carried out under the US-Israel Rotorcraft Project Agreement for cooperative research. The research at Penn State was partially funded by the U.S. Government under Agreement No. W911W6-17-2-0003. The U.S. Government is authorized to reproduce and distribute reprints for Government purposes notwithstanding any copyright notation thereon. The views and conclusions contained in this document are those of the authors and should not be interpreted as representing the official policies, either expressed or implied, of the U.S Government

## REFERENCES

1. "Multiservice Helicopter Sling Load: Single Point Rigging Procedures", U. S. Department of the Army TM 4-48.10, July, 2013
2. Raz, R., Rosen, A, Carmeli, A., Lusardi, J., Cicolani, L.S., Robinson, D., "Wind Tunnel and Flight Evaluation of Passive Stabilization of a Cargo Container Slung Load", *Journal of the American Helicopter Society*, Vol. 55, 03201, 2010, pp. 03200-1-18.
3. Raz, R., Rosen, A., Cicolani, L. S., and Lusardi, J., "Using Wind Tunnel Tests for Slung Loads Clearance - Part 1 – The CONEX Cargo Container", *Journal of the American Helicopter Society*, Vol.59, No.4, 2014, 042003-1-12.
4. Raz, R., Rosen, A., Cicolani, L. S., and Lusardi, J., Gassaway, B., and Thompson, T., "Using Wind Tunnel Tests for Slung Loads Clearance - Part 2 – Other Loads", *Journal of the American Helicopter Society*, Vol.59, No.4, 2014, 042004-1-12.
5. Watkins, T. C., Sinacori, J. D., Kesler, D. F., "Stabilization of Externally Slung Helicopter Loads," USAAMRDL TR 74-42, August, 1974.
6. Matheson, N., "The Stability of Portable Bridges Carried on Slings Beneath Helicopters," Australian Department of Defense Aerodynamics Report 154, January 1980.
7. Nyren, D., Tardiff, M., Desabrais, K., "Passive Stabilization and Stability Quantification of Helicopter Sling Load Payloads," Proceedings of the 71st Annual Forum of the American Helicopter Society, Virginia Beach, VA, May 5-7, 2015.
8. Cicolani, L. S., Ivler, C., Ott, C., Raz, R. and Rosen, A., "Rotational Stabilization of Cargo Container Slung Loads", Journal of the American Helicopter Society, Vol.60, No.4, 2015, 042006-1-13.
9. Enciu, K., and Rosen, A., "Simulation of Coupled Helicopter - Slung Load – Pilot Dynamics", *Journal of the American Helicopter Society*, Vol.62, No.1, 2017, 012007-1-13.
10. Ronen, T., "Dynamics of a Helicopter with a Sling Load," PhD thesis, Department of Aeronautics and Astronautics, Stanford University, Palo Alto, CA, 1985.
11. Miller, D., G., Lu, Y., White, F., Osciak, E, M., Roberts, B., Price, R., Wiedorn J., "Flight Simulation As A Tool To Develop V-22 Slung Load Capabilities," Proceedings of 55th Annual Forum of the American Helicopter Society. Montreal, Canada, 1999.
12. Tyson, P. H., "Simulation Validation and Flight Prediction of UH-60 Black Hawk Slung-Load Characteristics," MSc thesis, Naval Postgraduate School, Monterey, CA., March 1999
13. Raz, R., Fogel, O., Rosen, A., Berrios, M.G., and Cicolani, L. S., "Using Wind Tunnel Tests to Investigate Dual Lift Trim, Maneuvers, Stability and Control", Proceedings of the AHS International 73rd Annual Forum & Technology Display, Fort Worth, Texas, USA, May 9-11, 2017.
14. Dukes, T. A., "Maneuvering Heavy Sling Loads near Hover, Part I: Damping the Pendulous Motion," Journal of the American Helicopter Society, Vol. 18,(3), 1973, pp. 2-11.
15. Gamett, T.S., Jr., Smith, J.H., Lane, R., "Design and Flight Test of the Active Arm External Load Stabilization System," Proceedings of the American Helicopter Society 32nd Annual Forum, Washington D.C., May 10-12 1976.
16. Krishnamurthi, J., and Horn, J. F., "Helicopter Slung Load Control Using Lagged Cable Angle Feedback," Journal of the American Helicopter Society, Vol. 60, (2), 2015, pp. 1-12.
17. Ivler, C., "Design and Flight Test of a Cable Angle Feedback Control System for Improving Helicopter Slung Load Operations At Low Speed," RDMR-AF-14-01, April 2014.
18. Scaramal, M., Enciu, J., and Horn, J. F.," Active Stabilization of Slung Loads in High-Speed Flight Using Cable Angle Feedback", Journal of the American Helicopter Society, Vol. 64, 042008, 2019, pp. 1-12.
19. Patterson, B. W., Ivler, C., Hayes, P. M., "External Load Stabilization Control Laws For An H-6 Helicopter Testbed," Proceedings of the 70th Annual Forum of the American Helicopter Society, Montreal, Quebec, Canada, May 20-22, 2014
20. Patterson, B. W., Enns, R., King, C., Kashawlic, B. E., Mohammed, S., and Lukes, G., "Design and Flight Test of a Hybrid External Load Stabilization System for an H-6 Helicopter Testbed," American Helicopter Society 71st Annual Forum, Virginia Beach, Virginia, May 5-7, 2015.
21. Enciu, J., Singh, A., and Horn, J. F.," Stabilization of External Loads in High Speed Flight Using an Active Cargo Hook," 43rd European Rotorcraft Forum, Milan, Italy, September 12-15, 2017.
22. Singh, A., Enciu, J. and Horn, J. F.," Slung Load Stabilization Across the Flight Envelope Using an Active Cargo Hook," AIAA Scitech 2019 Forum, San Diego, California, 7-11 January 2019.
23. Tischler, M. B., Remple, R. K., *Aircraft and Rotorcraft System Identification*. Second Ed., American Institute of Aeronautics and Astronautics, Inc., 2012.
24. Bisgaard, M., la Cour-Harbo, A., and Bendsten J.D., "Swing Damping for Helicopter Slung Load Systems Using Delayed Feedback," AIAA Guidance, Navigation, & Control Conference, Chicago, IL, August 10-13, 2009.
25. Tischler, M.B., Berger, T., Ivler, C. M., Mansur, M. H., Cheung, K. K., Soong, J. Y., *Practical Methods for Aircraft and Rotorcraft Flight Control Design*, American Institute of Aeronautics and Astronautics, Inc., 2017.